Bioorganic Chemistry 145 (2024) 107227

Contents lists available at ScienceDirect

Bioorganic Chemistry

journal homepage: www.elsevier.com/locate/bioorg

The antimicrobial potential of adarotene derivatives against *Staphylococcus aureus* strains

Salvatore Princiotto [a,1], Bruno Casciaro [b,1], Alvaro G. Temprano [c,d,1], Loana Musso [a], Francesca Sacchi [a], Maria Rosa Loffredo [b], Floriana Cappiello [b], Federica Sacco [e], Giammarco Raponi [e], Virginia Perez Fernandez [f], Teresa Iucci [f], Maria Luisa Mangoni [b], Mattia Mori [c], Sabrina Dallavalle [a,*], Claudio Pisano [f]

[a] *Department of Food, Environmental and Nutritional Sciences, Università degli Studi di Milano, via Celoria 2, 20133 Milano, Italy*
[b] *Laboratory affiliated to Istituto Pasteur Italia-Fondazione Cenci Bolognetti, Department of Biochemical Sciences, Sapienza University of Rome, 00185 Rome, Italy*
[c] *Department of Biotechnology, Chemistry and Pharmacy, University of Siena, Via Aldo Moro 2, 53100 Siena, Italy*
[d] *Experimental Hepatology and Drug Targeting (HEVEPHARM) Group, Biomedical Research Institute of Salamanca (IBSAL), University of Salamanca, 37007 Salamanca, Spain*
[e] *Department of Public Health and Infectious Diseases, Sapienza University of Rome, 00185 Rome, Italy*
[f] *Special Products Line, 03012 Anagni, FR, Italy*

ARTICLE INFO

Keywords:
Antimicrobials
Staphylococcus aureus
Adarotene analogues
Membrane permeabilization
Molecular dynamics

ABSTRACT

Multidrug-resistant (MDR) pathogens are severely impacting our ability to successfully treat common infections. Here we report the synthesis of a panel of adarotene-related retinoids showing potent antimicrobial activity on *Staphylococcus aureus* strains (including multidrug-resistant ones). Fluorescence and molecular dynamic studies confirmed that the adarotene analogues were able to induce conformational changes and disfunctions to the cell membrane, perturbing the permeability of the phospholipid bilayer. Since the major obstacle for developing retinoids is their potential cytotoxicity, a selected candidate was further investigated to evaluate its activity on a panel of human cell lines. The compound was found to be well tolerated, with IC_{50} 5–15-fold higher than the MIC on *S. aureus* strains. Furthermore, the adarotene analogue had a good pharmacokinetic profile, reaching a plasma concentration of about 6 μM after 0.5 h after administration (150 mg/kg), at least twice the MIC observed against various bacterial strains. Moreover, it was demonstrated that the compound potentiated the growth-inhibitory effect of the poorly bioavailable rifaximin, when used in combination. Overall, the collected data pave the way for the development of synthetic retinoids as potential therapeutics for hard-to-treat infectious diseases caused by antibiotic-resistant Gram-positive pathogens.

1. Introduction

Bacterial resistance to antimicrobial drugs is one of the biggest threats to human health. Several clinically relevant organisms are rapidly evolving towards multidrug- and even pandrug-resistant phenotypes, whose global spread represents a significant Public Health issue [1]. It has been estimated that if the phenomenon is not controlled, more than 10 million people worldwide will die from multiple antibiotic resistance by 2050 [2]. It is therefore clear that novel antimicrobial drugs counteracting the development of bacterial resistance shall be considered as a critical priority [3]. Such a background is further exacerbated by a pronounced innovation gap in antimicrobial development, after the "golden era of antibiotic drug discovery". The lack of new efficient antibiotics has caused an imbalance in the permanent race between bacterial evolution and the protection of human health, leading to serious concerns of a fallback into a pre-antibiotic era.

In recent years we have focused our efforts on the investigation of compounds containing the adarotene skeleton (**1**, Fig. 1) as potential antimicrobials active on multidrug-resistant strains (MDR) [4].

To shed light on the molecular determinants responsible for bioactivity, a panel of adarotene-related retinoids were synthesized. Structural modifications were introduced on key portions of the parent

* Corresponding author.
E-mail address: sabrina.dallavalle@unimi.it (S. Dallavalle).
[1] These authors share first authorship and have contributed equally.

https://doi.org/10.1016/j.bioorg.2024.107227
Received 22 December 2023; Received in revised form 13 February 2024; Accepted 16 February 2024
Available online 18 February 2024

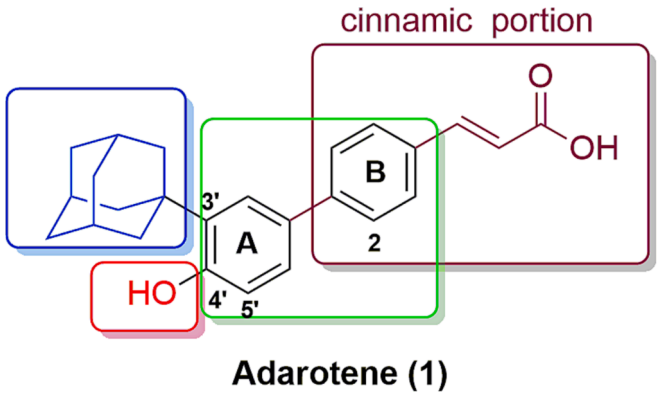

Fig. 1. Structure of adarotene (**1**).

compound, e.g. the phenolic OH, the lipophilic adamantyl group, the aromatic rings A and B, the conjugated double bond and the carboxylic acid moiety (Fig. 1). The replacement of the lipophilic bulky adamantyl group as well as the introduction of substituents on the phenolic OH were deleterious, causing a decrease in activity. Conversely, the introduction of substituents on the double bond and on the backbone maintained - and in some cases increased – the activity, even in the presence of quite bulky groups [4]. In particular, featuring ring B with lipophilic groups in position 2 gave potent antimicrobial compounds with bactericidal effect. The promising results prompted us to deepen the investigation, widening the coverage of the chemical space in the portion of the molecule most suitable for modification, i.e. the cinnamic moiety (Fig. 1). Specifically, we modulated the pattern of substitution on ring B and on the acrylic portion, maintaining in most cases the substitution pattern on ring A (Fig. 2). In this manuscript we report the results of this in-depth study, which support the potential of synthetic retinoids as promising chemotypes for the treatment of Gram-positive bacterial

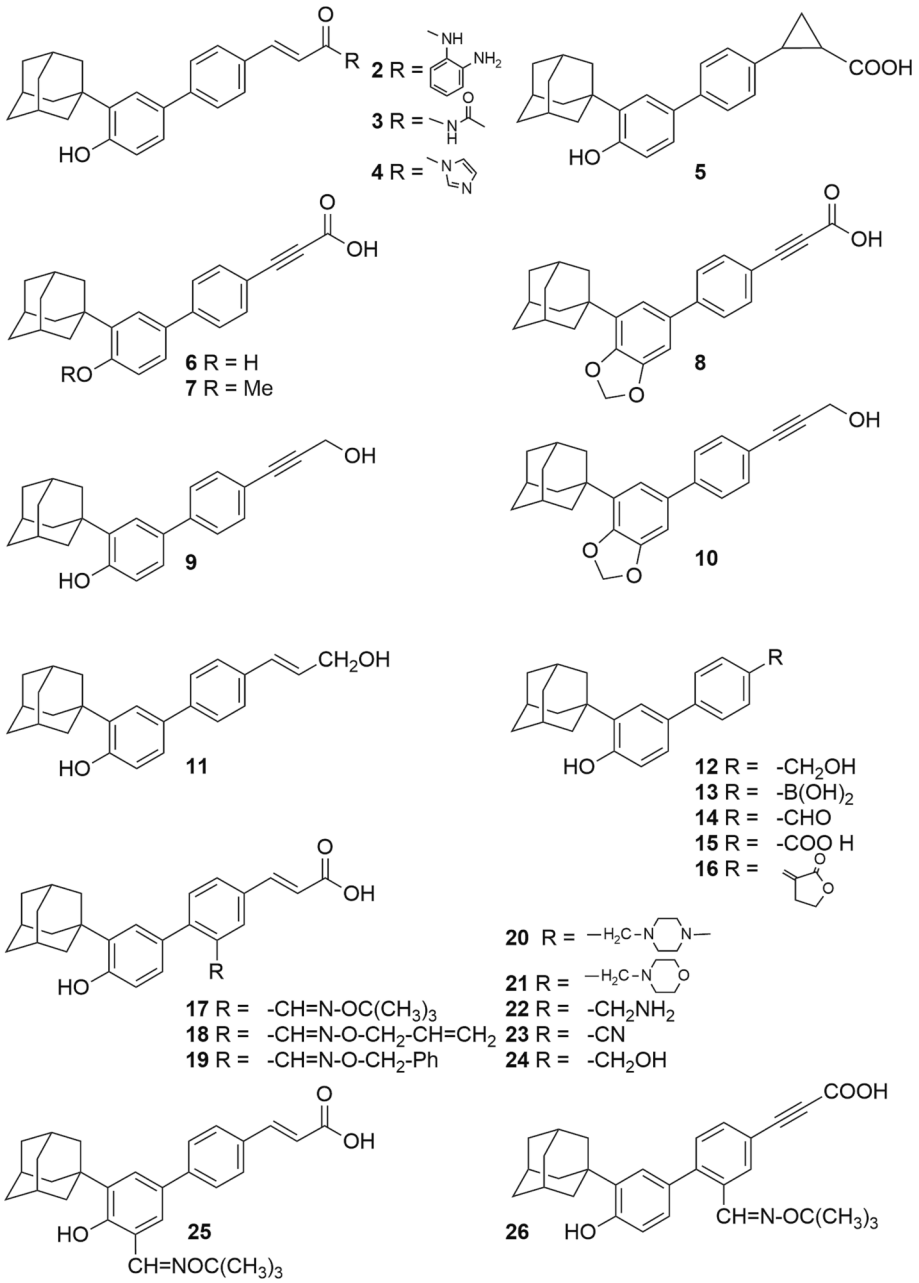

Fig. 2. Structures of adarotene analogues.

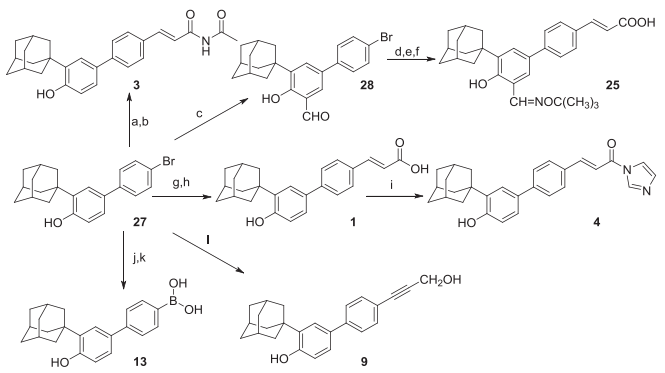

Scheme 1. Reagents and conditions: a) acrylonitrile, tri(*o*-tolyl)phosphine, Pd(OAc)$_2$, 45 %; b) acetic anhydride, PTSA, 2 h, 80 °C, 53 %; c) $(CH_2O)_n$, $SnCl_4$, 2,6-lutidine, toluene, 7 h, 95 °C, 60 %; d) Pd(OAc)$_2$, tri(*o*-tolyl)phosphine, Et_3N, *t*-butyl acrylate, 110 °C, 4 h, 60 %; e) *O*-*t*-butyl hydroxylamine hydrochloride, pyridine, EtOH, 2 h, reflux, quant.; f) TFA, dry CH_2Cl_2, 0 °C, 2 h, 95 %; g) methyl acrylate, tri(*o*-tolyl)phosphine, Pd(OAc)$_2$, TEA, 98 %; h) LiOH·H_2O, THF/H_2O, 94 %; i) CDI, DMF, 24 h, rt, 20 %; j) bis(pinacolato)diboron, KOAc, $PdCl_2$(dppf)·CH_2Cl_2, DMF, 6 h, 80 °C; k) CH_3COONH_4, acetone: H_2O 2:1, $NaIO_4$, 18 h, rt, 96 %; l) i. CuI, $PdCl_2(Ph_3P)_2$, diisopropylamine, TEA, 30 min., rt; ii. propargyl alcohol, 20 h, 60 °C, 19 %.

infections.

2. Results and discussion

2.1. Chemistry

Compounds **2**, **5**–**8**, **11**, **14**–**17**, **21**–**24** were prepared according to literature procedures [5–9]. Adarotene analogues **3**–**4**, **9**, **13** and **25** were synthesized starting from the common precursor **27** [5]. Compound **3** was obtained by Heck reaction of **27** with acrylonitrile, followed by treatment with acetic anhydride and PTSA at 80 °C. Oxime **25** was obtained by formylation of **27** to obtain **28**, which in turn underwent Heck reaction with *t*-butyl acrylate followed by reaction with *O*-*t*-butylhydroxylamine hydrochloride and final hydrolysis with TFA. Compound **4** was prepared from adarotene **1**, obtained from **27** following a previously reported procedure [5], by reaction with CDI. Compound **27** was converted into boronic acid **13** by reaction with bis(pinacolato)diboron, followed by reaction with $NaIO_4$. Finally, Sonogashira coupling of **27** with propargyl alcohol gave compound **9** (Scheme 1). Alcohol **12** was obtained by reduction of aldehyde **14** [5]. The precursor **29** was used to synthesize alcohol **10**, by Suzuki coupling with compound **31**, after the conversion into the corresponding protected boronate **30**. Compound **32** [5] was used to prepare the oximes **18** and **19** by reaction with suitable hydroxylamines. The same intermediate **32** was used to synthesize alkyne **26** through the formation of the dibromo derivative **33**, as previous attempts to prepare the compound by Sonogashira couplings were all unsuccessful (Scheme 2).

2.2. Biological activity evaluation

2.2.1. Antimicrobial activity

The synthesized compounds were tested on two representative bacteria, the Gram-positive *Staphylococcus aureus* ATCC 25923 and the Gram-negative *Escherichia coli* ATCC 25922 by determining the minimum inhibitory concentration (MIC). The corresponding values are reported in Table 1.

The results showed that the tested compounds were inactive against *E. coli*. Regarding *S. aureus*, derivatives **2**–**4**, having different moieties in place of the carboxylic acid group, displayed a decreased activity compared to the parent compound (MIC > 128 μM). On the contrary, the

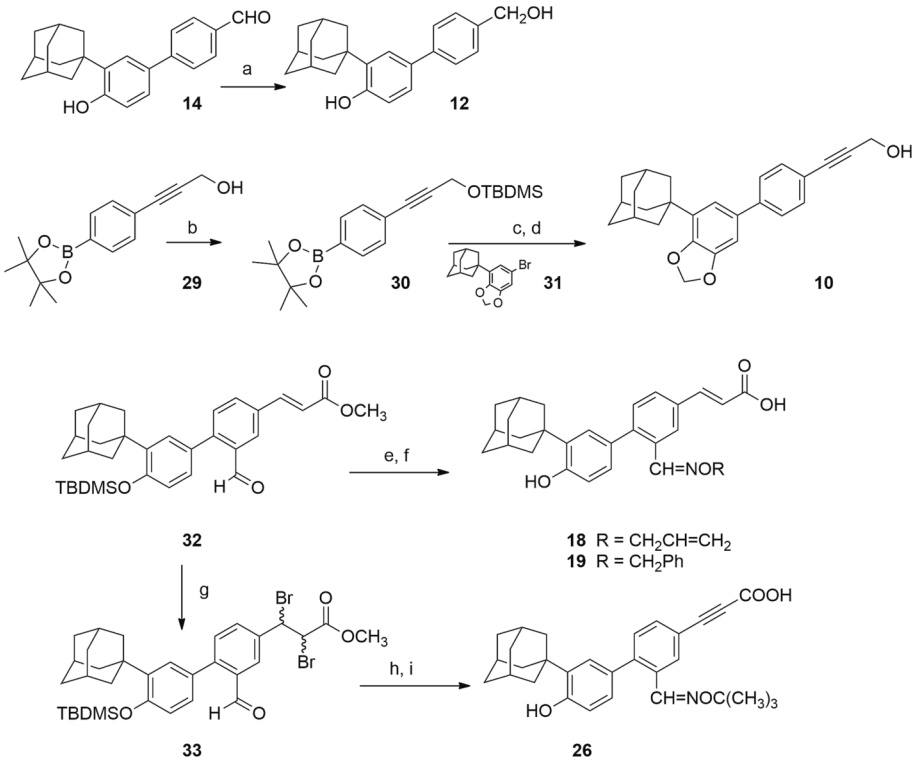

Scheme 2. Reagents and conditions: a) $NaBH_4$, MeOH, 30 min, rt, 60 %; b) TBDMSCl, dry DMF, imidazole, 0 °C then 2 h at rt, 51 %; c) **31**, dry dioxane, 2 M aq. Na_2CO_3, $PdCl_2$(dppf)·CH_2Cl_2, 3 h, reflux, 31 %; d) 1 M TBAF in THF, dry THF, 30 min, rt, 30 %; e) R-ONH_2·HCl, pyridine, for **18**: (R = –$CH_2CH=CH_2$), 4 h reflux, 94 % and for **19** (R = -CH_2Ph), 4 h reflux, 56 %; f) i. 1 M NaOH in CH_3OH, ii. 1 M HCl, for **18**: (R = –$CH_2CH=CH_2$), 2 h reflux, 85 % and for **19** (R = -CH_2Ph), 3 h reflux, quantitative; g) pyridinium tribromide, DCM, rt, 4 days, 79 %; h) *O*-*t*-butylhydroxylamine hydrochloride, EtOH, pyridine, 2 h, reflux, 65 %; i) KOH, isopropanol, 12 h, reflux, 30 %.

Table 1
Antimicrobial activity of compounds **1**–**26** expressed as MIC (μM) against two representative Gram-positive and Gram-negative strains (i.e., *S. aureus* ATCC 25923 and *E. coli* ATCC 25922, respectively). Ciprofloxacin (CIP) was used as positive control.

	MIC (μM)		
Cpd	*S. aureus* ATCC 25923		*E. coli* ATCC 25922
1	21		n.d.
2	>128		>128
3	>128		>128
4	>128		>128
5	64	>128	
6	16		>128
7	64		n.d.
8	16		>128
9	4		>128
10	>128		>128
11	16		>128
12	8		>128
13	4		>128
14	>128		>128
15	>128		>128
16	>128		>128
17	4 [4]		>128
18	4		>128
19	8		>128
20	32		>128
21	32		>128
22	>128		>128
23	>128		>128
24	128		>128
25	>128		>128
26	8		>128
CIP	1.5		0.023

n.d: not determined.

introduction of a cyclopropyl and a triple bond instead of the double bond in the cinnamic portion (compounds **5** and **6**, respectively) did not turn out to be deleterious (MIC = 64 μM for compound **5** and 16 μM for compound **6**). The significant activity shown by the alkyne **6** prompted us to synthesize the corresponding derivatives with a methoxy group and a methylenedioxy group masking the phenolic OH (compounds **7** and **8**, respectively). The introduction of the methoxy group (compound **7**) reduced the activity, which was however maintained in compound **8**.

In addition, analogues with a primary alcohol in place of the carboxylic group (compounds **9** and **10**) were prepared. Interestingly, compound **9** had a MIC = 4 μM, whereas compound **10** turned out to be inactive (MIC > 128 μM). This strong difference in terms of activity highlighted the key role of the phenolic group, which was confirmed by the MD studies (see below). As the introduction of a hydroxy group seemed rather promising, the cinnamyl alcohol **11** was prepared (MIC = 16 μM). Removal of the double bond gave a compound with the alcohol group directly installed on the aromatic ring (**12**). Surprisingly, the activity was not lost (MIC = 8 μM). Therefore, other compounds with a small polar group directly bound to the B ring were investigated (**13**–**16**). Compound **13** displayed a MIC = 4 μM, while compounds **14**, **15** and **16** were not active (MIC > 128 μM). The attention was then turned to ring B-substituted compounds. Compound **17**, with MIC = 4 μM against *S. aureus* [4] had a *t*-butyl oxime on carbon 2. Two further oximes with lipophilic groups in position 2 were prepared (compounds **18** and **19**), showing an antimicrobial activity comparable to that of **17** (MIC = 4 and 8 μM, respectively).

Polar moieties such as methylpiperazine, morpholine and amine groups were introduced at the same position (compounds **20**, **21**, **22**, with MIC values of 32, 32 and >128 μM, respectively) confirming that a protonatable group was deleterious for the activity. Derivatives with a cyano and an alcohol group were also prepared (compounds **23** and **24**), showing however poor antibacterial activity (MIC > 128 μM and 128 μM, respectively). Eventually, the substituent found in compound **17** was shifted to ring A (compound **25**) to assess the effect of the position of the groups on the biphenyl skeleton. This change caused a loss of activity (MIC > 128 μM). Finally, a compound incorporating into the same molecule the most promising modifications (triple bond and oxime in position 2) was synthesized (compound **26**) and tested, showing a MIC = 8 μM.

Based on the obtained results, compound **17**, its structurally related analogues **18** and **19** and compound **9** were selected for further investigation, expanding the panel of Gram-positive strains to include multidrug-resistant clinical isolates (Table 2).

As reported in Table 2, compound **17** retained its antimicrobial activity (MIC in the range 2–4 μM) against *S. epidermidis* ATCC 12228 and, interestingly, also against multidrug-resistant *S. aureus* strains. The other tested compounds showed a comparable or weaker activity with MIC ranging from 4 to 64 μM.

Table 2
Antimicrobial activity of compounds **9**, **17**, **18** and **19** expressed as MIC (μM) against a panel of *Staphylococcus* strains, including multidrug-resistant ones.

		MIC (μM)			
Strain	**Resistance profile**	**9**	**17**	**18**	**19**
S. epidermidis ATCC 12228	–	8	4	8	4
S. aureus ATCC 43300	MET - OXA	64	2	8	4
S. aureus #2	BEN - CLI - DAP - ERI - LEV - OXA -VAN	8	4	8	16
S. aureus 13667073	AZI - BEN - CIP - CLI - ERI - LEV - MOX - OXA	16	4	8	4
S. aureus 0216108	BEN - CIP - LEV - MOX - OXA	16	2	8	4

MET, methicillin; OXA, oxacillin; BEN, benzylpenicillin; CLI, clindamycin; DAP, daptomycin; ERI, erythromycin; LEV, levofloxacin; VAN, vancomycin; AZI, azithromycin; CIP, ciprofloxacin; MOX, moxifloxacin

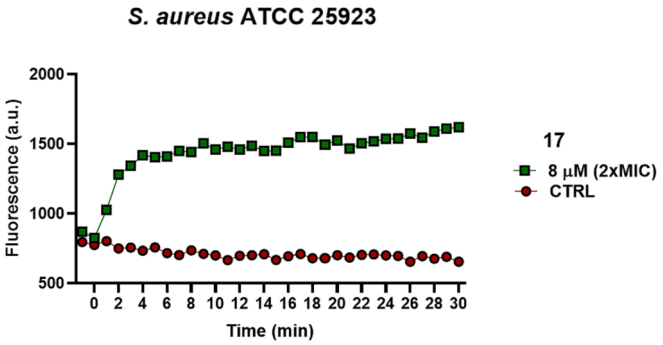

Fig. 3. Kinetics (0–30 min) of membrane permeabilization of *S. aureus* ATCC 25923 induced by the addition of compound **17** (time = 0) at 8 μM. Samples were incubated with 1 μM SYTOX Green and changes in fluorescence were monitored in a microplate reader. Controls (CTRL) were microbial cells treated with vehicle. Values correspond to one representative experiment of three. (For interpretation of the references to colour in this figure legend, the reader is referred to the web version of this article.)

2.2.2. Membrane permeabilization

Previous studies reported that the antimicrobial activity of adarotene analogues was due to their ability to penetrate and embed in lipid bilayers [4,10]. The membrane-disruptive action of retinoid-related molecules could be partially attributed to the interaction with the membrane components, which eventually results in membrane conformational changes and dysfunction, leading to cell death.

Hypothesizing the membrane perturbing activity as the major mechanism of the bactericidal activity, the rate of bacterial killing should be fast and concomitant with the membrane perturbation. Therefore, we evaluated the membrane-perturbation kinetics by using a fluorescence-based assay with the membrane impermeant probe SYTOX

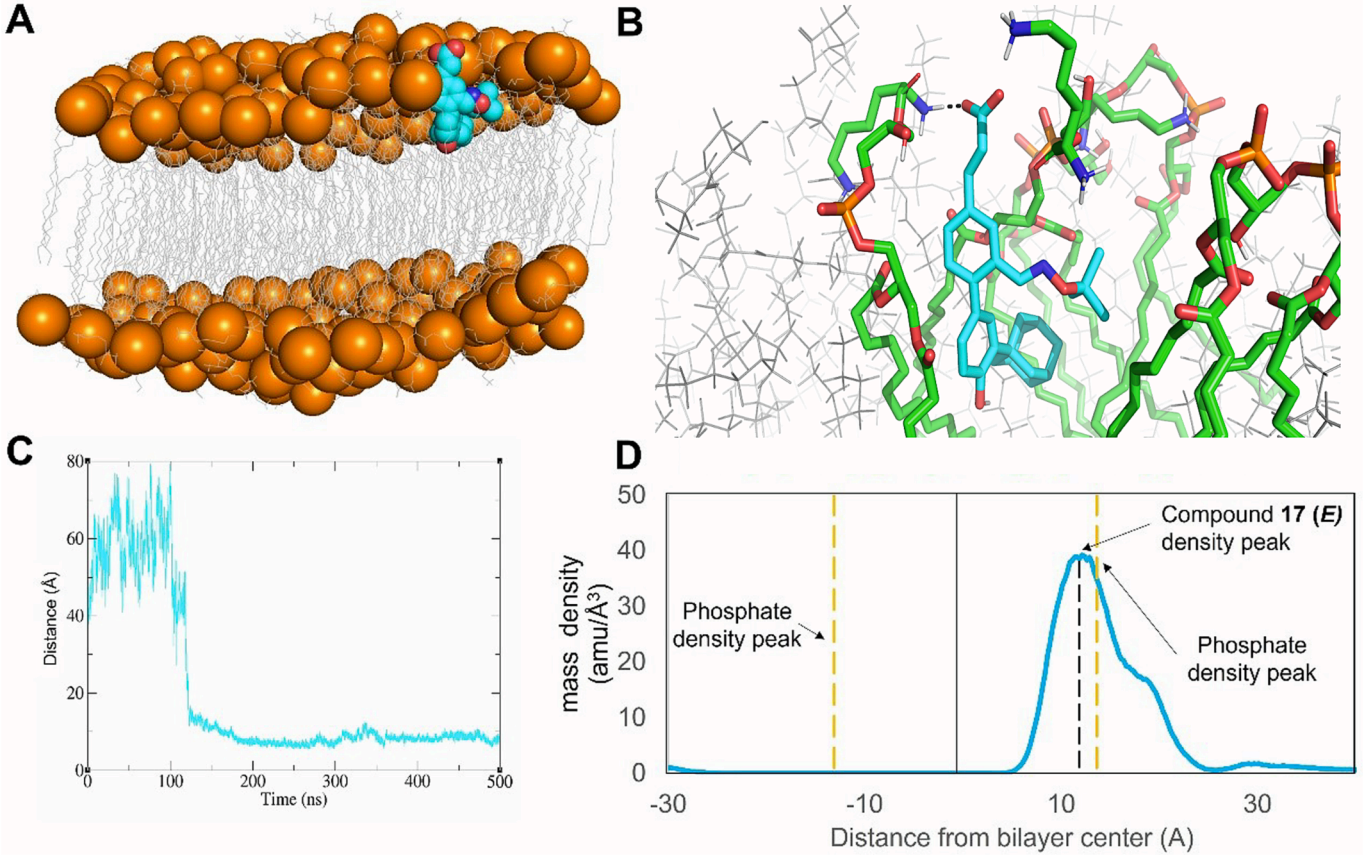

Fig. 4. A: Representative snapshot extracted from MD trajectories (500 ns – the representative frame of the most populated cluster is shown) describing the membrane/**17(*E*)** interaction. The ligand is shown as cyan spheres, while phospholipids are represented as grey lines, with their phosphorous atoms highlighted as orange spheres; **B**: magnification of the interaction between **17(*E*)** (cyan sticks) with the membrane residues within 5 Å from the compound (shown as green sticks), the polar interaction is highlighted by a black dashed line; **C**: plot of the distance between **17(*E*)** and its binding site on the *S. aureus* membrane along MD trajectories; **D**: mass density profile of **17(*E*)** with the corresponding peak highlighted by black dash line. The density peaks of the lipid phosphate groups are indicated with orange dashed lines. Maximums of mass density in membrane are at −13.125 Å and 13.625 Å. (For interpretation of the references to colour in this figure legend, the reader is referred to the web version of this article.)

Green. This probe enhances its fluorescence when bound to nucleic acids, but it is not able to cross the membrane of intact cells. Following the addition of a compound capable of rapidly perturbing the cytoplasmic membrane, the binding of the probe to the intracellular nucleic acids leads to a fast increase in the fluorescence signal, as reported in Fig. 3. When compound **17** was added to the bacterial cells at the concentration of 8 μM a sharp increase of fluorescence intensity was recorded, reaching a plateau within the first 4 min. This is in line with the concomitant bacterial death which was 98.7 % (±1.12) after 30 min. In contrast, no fluorescence signal and no bacterial death were observed for the control samples.

These results support the hypothesis that the class of adarotene derivatives is able to perturb the cell membrane, with consequent increased membrane permeability and bacterial death, in agreement with the results reported by Kim et al. [10].

The capability of compound **17** to permeabilize bacterial membranes was also evaluated against another *Staphylococcus* strain, i.e. *S. epidermidis* ATCC 12228 by means of the SYTOX Green assay and HPLC method (Figs. S5 and S6).

2.2.3. Investigation of the interaction with the bacterial membrane via MD simulations

To probe the interaction of adarotene derivatives with the bacterial membrane, and to monitor how structural modifications can influence their ability to embed within the target, a symmetric pure lipid bilayer membrane system of *S. aureus* was built using the CHARMM-GUI Membrane Builder tool [11,12]. The phospholipid composition of the lipid bilayer in the simulations was adapted from previous molecular dynamics (MD) studies of membrane-containing systems [10,13–15]. To check whether the membrane model is geometrically stable, MD simulations were run. The root-mean-squared deviation (RMSD) of the membrane was calculated, showing that the structure achieves conformational stability after 70 ns of MD simulation (Fig. S7). The mass density of the membrane along MD trajectories shows a stable distribution of the phospholipids and the solvent, including water molecules and ions (Fig. S8). To further validate the membrane model, the interaction of the positive control **CD437**, i.e., an adarotene analogue that has been found to impair *S. aureus* growth through membrane interaction by Kim *et al.* [10], was simulated. MD simulations confirmed the ability of **CD437** to bind the *S. aureus* membrane, as described in the original publication [10] (Figs. S9-S10) with the retinoid penetrating the bilayer and becoming embedded orthogonally to the lipid molecules in the membrane leaflet. With these results, we can conclude that the membrane model is suitable for studying the interaction of adarotene derivatives investigated herein.

The validated MD protocol was subsequently used to investigate the interaction of the most promising compound **17** and the selected adarotene analogues **9** and **10** with the *S. aureus* membrane model through 500 ns MD simulations with AMBER18 [16,17]. Compounds **9** and **10** were selected as they share a very high chemical similarity, although experiencing opposite effects against *S. aureus*. Indeed, compound **9** proved able to impair the growth of *S. aureus*, whereas compound **10**,

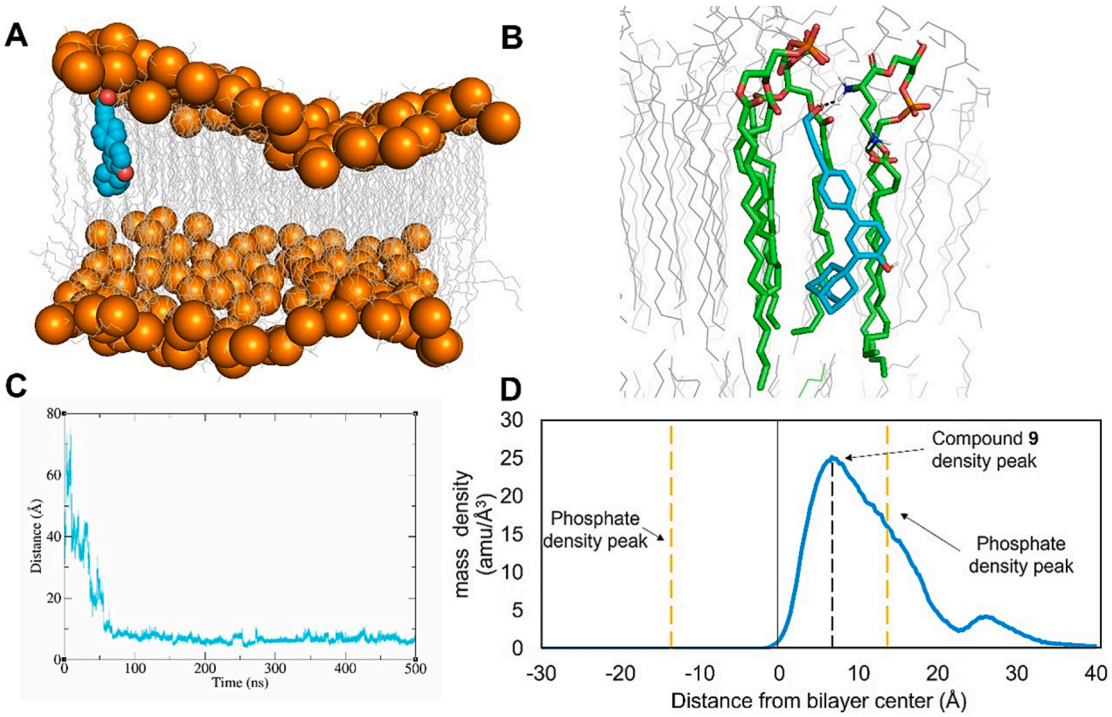

Fig. 5. A: Representative snapshot extracted from MD trajectories (500 ns – the representative frame of the most populated cluster is shown) describing the membrane/**9** interaction. The ligand is shown as cyan spheres, while phospholipids are represented as grey lines, with their phosphorous atoms highlighted as orange spheres; **B**: magnification of the interaction between **9** (cyan sticks) with the membrane residues within 5 Å from the compound (shown as green sticks). The hydrogen bond of 1.8 Å is highlighted by black dashed lines; **C**: plot of the distance between **9** and its binding site on the *S. aureus* membrane along MD trajectories; **D**: mass density profile of **9** with the corresponding peak highlighted by black dash line. The density peaks of the lipid phosphate groups are indicated with orange dashed lines. Maximums of mass density in membrane are at −13.375 Å and 12.875 Å. (For interpretation of the references to colour in this figure legend, the reader is referred to the web version of this article.)

which bears a methylenedioxy moiety in place of the phenolic OH group, resulted inactive. Accordingly, the compounds represent a suitable training set to probe the interaction with the *S. aureus* membrane via MD simulations, and to monitor how subtle changes in the structure of these molecules can influence their ability to embed within the target membrane.

Aldoxime **17** was isolated and chemically characterized as single diastereoisomer. Based on ROESY experiments and evidences from the literature [18,19] the compound in our hand was identified as the *E* isomer (see SI for details, Fig. S1-S4). Thus, MD simulations were performed on (*E*)-*t*-butoxyiminomethyl isomer, herein after referred to as **17(*E*)**.

The results showed a marked propensity of the molecule to bind the *S. aureus* membrane model. After about 70 ns of MD, compound **17(*E*)** initiated interaction with the membrane surface, resulted fully embedded in the membrane by the 100 ns (Fig. 4A-B), by establishing a hydrophobic interaction through its adamantyl moiety, as demonstrated by the distribution of the ligand mass density during MD simulations (Fig. 4D). Within the *S. aureus* membrane model, the carboxylic group is engaged in a salt bridge with the positively charged terminal of the Lys-PG unit, as highlighted in Fig. 4B. Noteworthy, the carboxylic group of **17(*E*)** is placed in a membrane region endowed with a predominance of protonated amino groups, suggesting that electrostatic interactions might play a role in membrane embedding of derivatives studied herein. This interaction model is maintained, on average, for the rest of the MD simulation. Notably, **17(*E*)** mass density shows a peak at around 12.375 Å from the bilayer center, which is below the density peak related to the lipid's phosphate groups, corresponding to about 13.625 Å. These results are consistent with the hypothesis that **17(*E*)** predominantly resides below the level of the lipids phosphate groups, and it is fully embedded in the lipidic bilayer. Since aldoximes could suffer from isomerization problems [18–20], we performed MD simulations with compound **17(*Z*)** as well, to make sure that the interaction with the membrane did not significantly change in the case of partial isomerization in *in vivo* systems. Luckily, compound **17(*Z*)** showed an analogous behaviour (Figs. S11, S12, and S13).

A very similar behaviour was observed for compound **9** as well. After about 70 ns of MD, compound **9** establishes a hydrophobic interaction with the membrane through its adamantyl moiety, while the alcoholic hydroxyl group establishes a H-bond interaction with the ammonium group of a Lys-PG unit, which further stabilizes the intermolecular adduct and allows a deeper penetration within the membrane (Fig. 5A-B), as demonstrated by the distribution of the ligand mass density during MD simulations (Fig. 5D). This interaction model is maintained, on average, for the rest of the MD simulation. Notably, **9** mass density shows a peak at around 6.625 Å from the bilayer center, which is below the density peak related to the lipid's phosphate groups, corresponding to about 12.875 Å. These results are consistent with the hypothesis that **9** predominantly resides below the level of the lipids phosphate groups, and it is fully embedded in the lipidic bilayer.

On the contrary, compound **10** shows less stable and weaker interactions with the phospholipid bilayer. In MD simulations, **10** mostly fluctuates in the solvent area in proximity of the membrane, without establishing interactions with the phospholipid heads that are strong enough to remain anchored to the membrane leaflet, as observed for **9**. Mass density analysis shows a ligand's peak at around 30 Å from the bilayer center (Fig. 6) which clearly indicates that the compound is outside the membrane. Based on these results, we assume that **10** presents less affinity for the lipid bilayer than its phenolic analogue **9**, which is consistent with the results obtained in the biological assays. Finally, as in the case of **17** (Fig. S14), we monitor whether the interaction of **9** and **10** with the membrane might induce conformational changes. As reported in Figs. S15 and S16, monitoring the RMSD of the ligand/membrane complexes along MD trajectories clearly shows that **9**

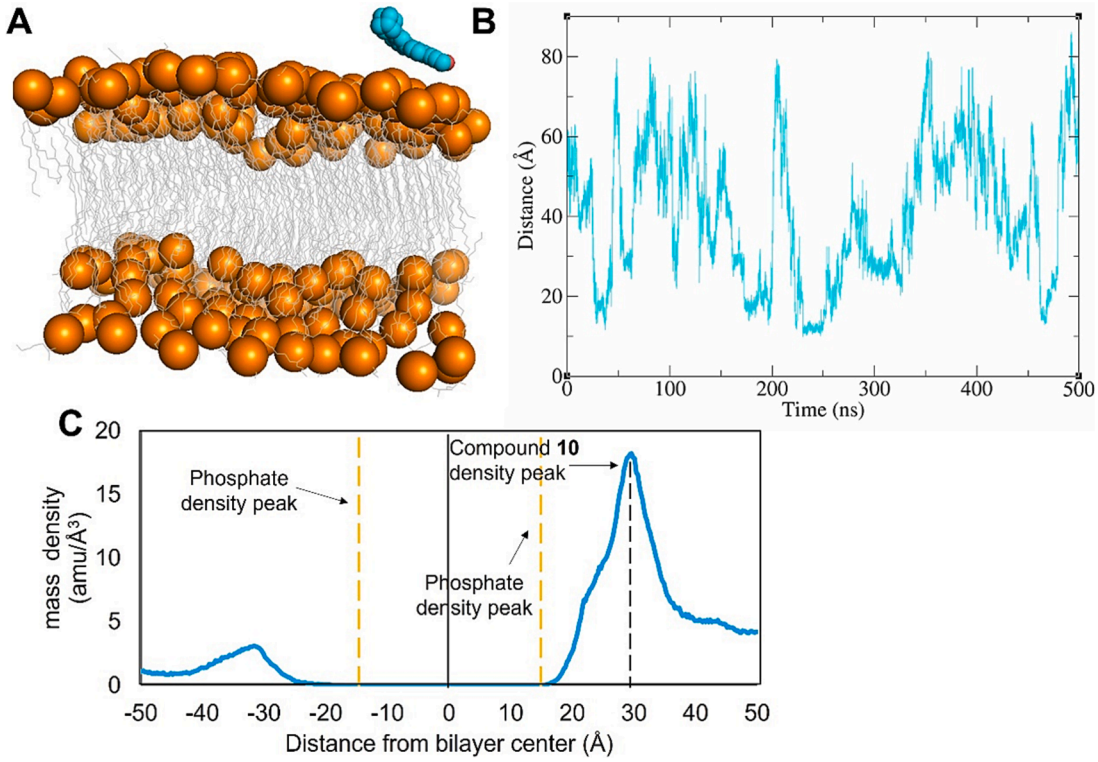

Fig. 6. **A**: Representative snapshot extracted from MD trajectories (500 ns – the representative frame of the most populated cluster is shown) describing the membrane/**10** interaction. The ligand is shown as cyan spheres, while phospholipids are represented as grey lines, with their phosphorous atoms highlighted as orange spheres; **B**: plot of the distance between **10** and the closest residues of the *S. aureus* membrane along MD trajectories; **C**: mass density profile of **10** with the corresponding peak highlighted by black dash line. The density peaks of the lipid phosphate groups are indicated with orange dashed lines. Maximums of mass density in membrane are at −13.375 Å and 12.875 Å. (For interpretation of the references to colour in this figure legend, the reader is referred to the web version of this article.)

significantly impairs the conformational stability of the *S. aureus* model membrane, whereas **10** does not, in agreement with experimental results. Overall, and in line with previous reports [10], MD simulations clearly suggest that the site of action of **9** and **17** might be the bacterial membrane of *S. aureus*, whose conformation is locally destabilized by the interaction with the small molecules.

With the aim to preliminarily evaluate if a ligand:membrane stoichiometry different than 1:1 might prevent or enhance the interaction of **9** with the *S. aureus* membrane model, a MD simulation with 2 molecules of **9** in the simulation box was carried out. Results of MD simulations were highly comparable to those obtained with a single molecule of **9**, both in terms of internalization and binding within the membrane, as also underlined by the mass density analysis (Fig. 7). Notably, the two molecules cluster together into a non-covalent dimer in the solvent area after around 240 ns of MD production (Fig. 7). A pi-stacking interaction of around 4 Å can be observed between the two compounds. Then, the homodimer of **9** interacts with the membrane thanks to the ability of the alcoholic hydroxyl groups to establish hydrogen bonds with phospholipids. The binding mode of the two **9** units is preserved till the end of the MD simulation. The dimer resides below the level of the lipid's phosphate groups, as demonstrated by the distribution of the compound mass density during the simulation, with respect to the bilayer.

The presence of the phenolic group in the adarotene analogues is essential to establish a proper interaction with the membrane, in agreement with previously observations by Wooseong Kim et al. [10]. Although being endowed with a higher hydrophobicity than **9**, the lack of the phenolic OH in **10** prevents the compound to penetrate the membrane and to establish profitable interactions with phospholipids. These results are consistent with *in vitro* results, further corroborating that the mode of action of the selected compounds **9** and **17** is related with their interaction with the *S. aureus* membrane.

2.2.4. Tolerability evaluation

Despite the potential advantages of the investigated membrane-active adarotene analogues – including fast killing and low probability of developing resistance – the major obstacle for developing retinoids as therapeutics is their potential cytotoxicity, which is a matter of debate [21].

For this reason, we evaluated the tolerability of selected compound **17**, which showed one of the best profiles of antimicrobial activity, on human cell lines. Specifically, the toxicity of the adarotene derivative was tested on HaCaT (immortalized human keratinocytes), human fibroblasts, AoSMC (Human Vascular Smooth Muscle Cells) and HUVEC (Human Umbilical Vein Endothelial Cells).

The results, reported in Table 3, showed that compound **17** tested at 2 μM concentration did not induce significative cell death. In fact, the percentage of survival of human cells was higher than 87 % for all the treated cell lines. The effect on the viability of human keratinocytes (HaCaT) and endothelial (HUVEC) primary cells was also evaluated at higher concentrations (20 μM), revealing that, even at these concentrations, the compound did not produce any toxic effect (Table 3).

We subsequently exposed human HaCaT cells to eight different concentrations (80, 40, 20, 10, 5, 2, 1 and 0.5 μM) for 24 h. For each concentration of the compound, eight replicates and the control (complete medium) were tested. The antiproliferative activity was assessed upon a further 48 h recovery in drug-free medium with the SRB assay. The results of this experiment showed no toxicity of compound **17** up to the highest concentration (80 μM) tested (Table S1).

2.2.5. Pharmacokinetic evaluation

The absolute values of plasma concentration at different time points and the corresponding graph of 17 kinetics were generated in female CD1 mice at doses of 50, 100, and 150 mg/kg, with blood samples

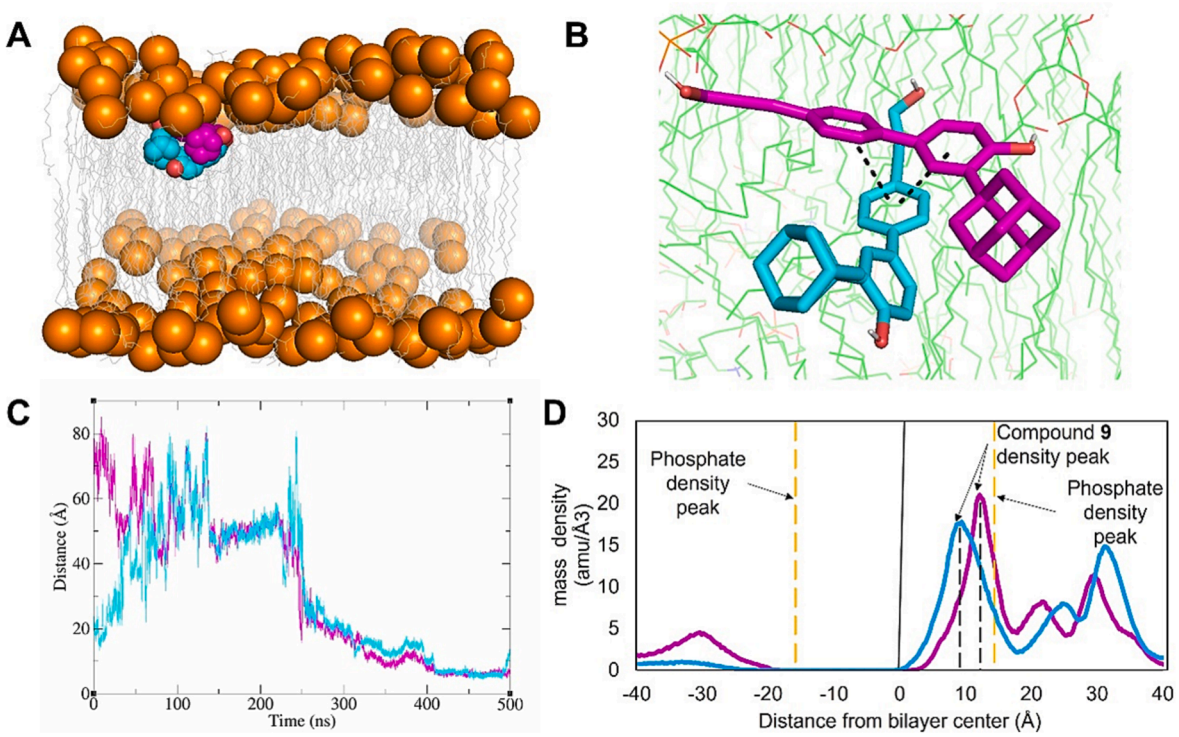

Fig. 7. A: Representative snapshot extracted from MD trajectories (500 ns – the representative frame of the most populated cluster is shown) describing the membrane/**9** interaction in a 1:2 stoichiometry. The ligand units are shown as cyan and magenta spheres, while phospholipids are represented as grey lines, with their phosphorous atoms highlighted as orange spheres; **B**: magnification of the interaction between the two **9** molecules (cyan and magenta sticks) with the membrane residues within 5 Å from the compounds (shown as green sticks). The pi-stacking interaction between **9** aromatic rings of around 4 Å is highlighted by black dashed lines; **C**: plot of the distance between each **9** molecule and their binding site on the *S. aureus* membrane along MD trajectories; **D**: mass density profile of each **9** molecule with the corresponding peak highlighted by black dash line. The density peaks of the lipid phosphate groups are indicated with orange dashed lines. Maximums of mass density in membrane are at −15.875 Å and 14.375 Å. (For interpretation of the references to colour in this figure legend, the reader is referred to the web version of this article.)

Table 3
Effect of fixed doses (2 μM) of 17 on the viability of fibroblasts and smooth muscle (AoSMC) and at two doses (2 and 20 μM) in human keratinocytes (HaCaT) and endothelial (HUVEC) primary cells.

	2 μM	20 μM
Cell line	**% Survival**	
HaCaT	109	99
Fibroblasts	88	–
AoSMC	99	–
HUVEC	88	97

Human primary cells were exposed to **17** for 24 h and cell survival assessed upon a further 48 h recovery in drug-free medium with the SRB assay. The relative viability of treated cells was expressed as percentage of untreated controls.

collected from 4 animals per time point (Fig. 8 and Table 4). Furthermore, the generated data underwent non-compartmental analysis, and the main parameters revealed that **17** has an average half-life (t/2) of approximately 6 h at all three doses, with a C_{max} of 2.91, 4.25, and 6.36 μM at the respective doses of 50, 100, and 150 mg/kg.

2.2.6. Combination with rifaximin

Rifaximin (RIF) is a poorly absorbed non-systemic antimicrobial agent used in various gastrointestinal disorders [22]. RIF is a rifamycin derivative with potent *in vitro* antimicrobial activity against Gram-positive and Gram-negative aerobic and anaerobic bacteria, especially against *Staphylococcus* spp., *Streptococcus* spp., *Enterococcus* spp., with MICs ranging from 0.015 to 2 μg/mL (40 nM to 8 μM). [23–26] RIF displays potent *in vivo* antimicrobial activity against enteropathogens, due to its extremely high luminal concentrations [27]. It is also structurally-related to rifampin, which is pivotal for the treatment of staphylococcal foreign body infections [28,29]. Considering that the close structural relationship of RIF to rifampin may lead to cross-resistance, it is important to explore combinatorial strategies favoring combination of different compounds to avoid mono-drug therapies. Different authors used rifaximin as selected antibiotic for combinatorial studies with diverse molecules. As examples: Betts and collaborators tested RIF in combination with polymyxins for selective decontamination of resistant bacteria in the human gut; [30] RIF is widely used in patients with hepatic encephalopathy in combination with lactulose; [31] Buldain et al tested RIF with *Melaleuca armillaris* essential oil against *Staphylococcus aureus* strains isolated from dairy cows. [32] Considering the clinical importance of this drug, we evaluated the capability of compound **17** to potentiate the growth-inhibitory effect of RIF when used in combination. In particular, compound **17** (at a concentration corresponding to half MIC) was combined with a sub-inhibitory concentration of RIF (1/2 MIC) and evaluated against *S. aureus* ATCC 25923 and a multidrug-resistant (MDR) strain of *S. aureus* (named #2 MDR). The microbial growth was monitored for 16 h at 37 °C in a microplate reader by measuring the absorbance of the microbial culture. As reported in Fig. 9 (Panel A and B), compound **17** was able to potentiate the effect of RIF in inhibiting *S. aureus* growth as proved by the slower growth curve of the combinations (green lines) versus that of the single drugs, when used at the corresponding concentrations (blue and yellow lines for compound **17** and RIF, respectively). Against *S. aureus* ATCC 25923, the combination of compounds was able to totally inhibit microbial growth after 14 h of treatment, while a start of microbial growth was recorded at 16 h. Against the clinical isolate, combination of both compounds was able to totally

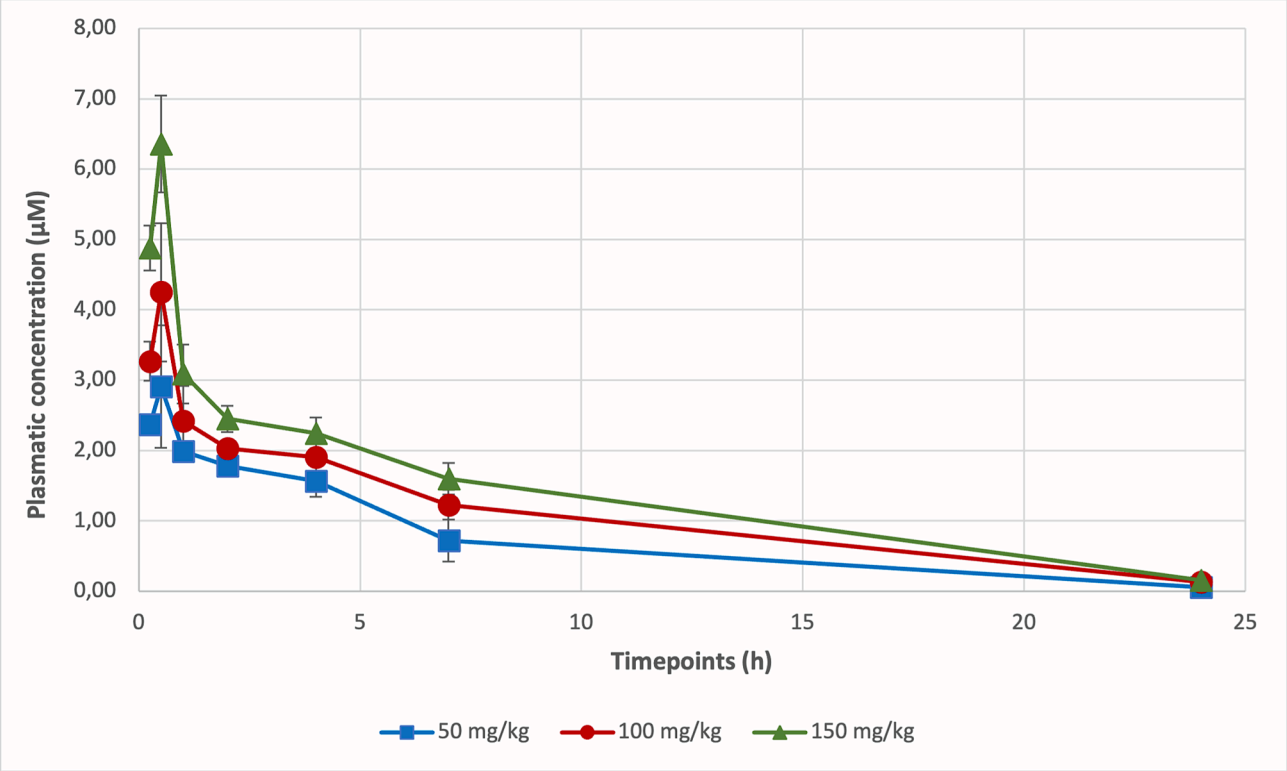

Fig. 8. Pharmacokinetics analysis of **17** at 50, 100 and 150 mg/kg administered by oral route in mice.

Table 4
Absolute values of plasma concentration after oral administration of **17** at different doses.

Dose (mg/kg)	Timepoints (hours)/Concentration (µM)*						
	0.25	**0.5**	**1**	**2**	**4**	**7**	**24**
50	2.37 ± 0.14	2.91 ± 0.87	1.99 ± 0.12	1.78 ± 0.15	1.57 ± 0.23	0.72 ± 0.30	0.06 ± 0.03
100	3.27 ± 0.28	4.25 ± 0.98	2.42 ± 0.50	2.03 ± 0.08	1.91 ± 0.11	1.23 ± 0.21	0.13 ± 0.04
150	4.88 ± 0.32	6.36 ± 0.69	3.09 ± 0.42	2.45 ± 0.19	2.25 ± 0.22	1.60 ± 0.22	0.16 ± 0.03

* plasma concentrations are expressed as the average plasma dosages of 4 animals /timepoints ± SD.

inhibit the microbial growth within 8 h of treatment, followed by a slowed microbial growth with respect to the control and the single compounds used alone. These results suggest that a combination of compound **17** and RIF is an effective strategy to enhance the efficacy of rifampin-derivatives in the treatment of chronic Gram-positive bacterial infections. This is because combination therapies can have important advantages: (i) reduction of the effective dose of both compounds; (ii) reduction of their possible cytotoxicity; (iii) reduction of the risk of the appearance of resistant phenotypes.

3. Conclusions

The pivotal work by Kim et al [10] paved the way for investigating synthetic retinoids as antimicrobials. We conducted a SAR study for this class of compounds expanding the coverage of the chemical space in the portion of the molecule most suitable for modification, i.e. the cinnamic moiety. Although limited, our analysis of structure–activity relationships showed that modifying the retinoid biphenyl core groups can result in improved antimicrobial profiles while reducing cytotoxicity. The shape of the molecules, together with the presence of key groups on the biphenyl backbone, were found to have a key role for the antimicrobial activity. We found that featuring ring B with lipophilic groups in position 2 gave potent antimicrobial compounds with low cytotoxic activity. Additionally, from our results it emerged that two polar groups and a quite rigid and compact skeleton could be important for membrane attachment and penetration.

This is in our opinion an important finding, since the major obstacle for developing retinoids as antimicrobials is their potential cytotoxicity. Gratifyingly, the selected candidate **17** was found to be well tolerated, with IC_{50} 5–15-fold higher than the MIC on *S. aureus* strains. Furthermore, the compound had a good PK profile, reaching a 6 µM plasma concentration after 0.5 h after administration, a concentration at least twice the MIC observed against various bacterial strains. The mode of action of the compounds was confirmed by membrane permeabilization studies and it was further corroborated by MD simulations on a lipid bilayer membrane systems of *S. aureus,* which was built to probe the interaction of the adarotene derivatives with the bacterial membrane. The model allowed us to monitor the effect of changes in the structure of the molecules on their ability to embed within the target, as well as to perturb the *S. aureus* membrane conformation, and could be useful in the future to identify new chemotypes with improved antimicrobial profile.

It is important to point out that, although our evidence emphasizes that the target of the studied compounds is the bacterial membrane, we cannot rule out other targets. This is a rather common issue with drugs and drug candidates.

Overall, the collected data confirmed that the scaffold of adarotene is a promising chemotype for further developments of non-toxic antimicrobials active on resistant strains. Our results warrant further development of synthetic retinoids as potential therapeutics for hard-to-treat infectious diseases caused by antibiotic-resistant Gram-positive pathogens.

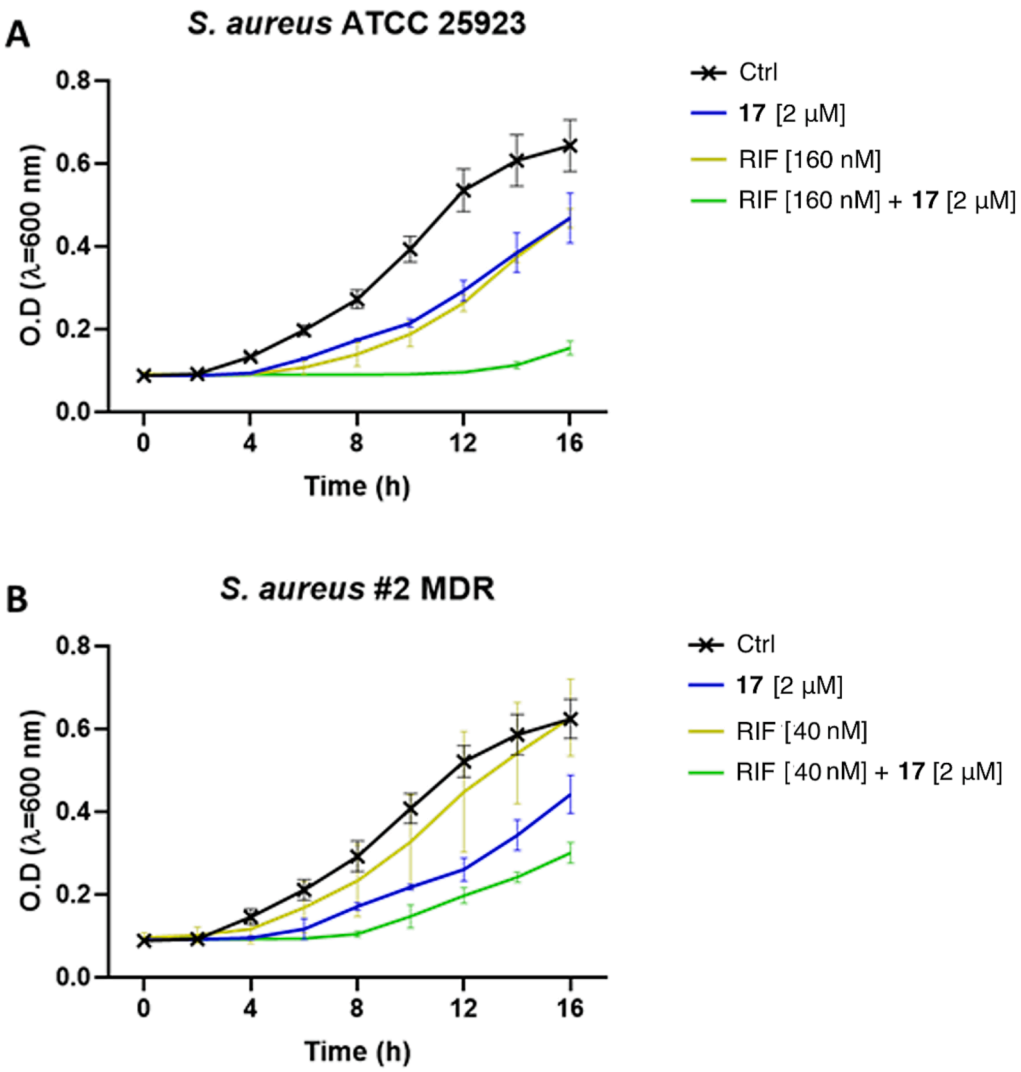

Fig. 9. Growth kinetics of (A) *S. aureus* ATCC 25923 and (B) *S. aureus* #2 MDR strains in the presence of rifaximin (RIF) at 1/2 MIC (yellow lines) in presence of compound 17 at its 1/2 MIC (2 μM, blue lines) as well as in the presence of their combinations (green lines). Results are the mean ± standard deviation (SD) of three independent experiments. (For interpretation of the references to colour in this figure legend, the reader is referred to the web version of this article.)

4. Experimental

4.1. Chemistry: general methods

All reagents and solvents were reagent grade or were purified by standard methods before use. Melting points were determined in open capillaries by an SMP3 apparatus and are uncorrected. ^{1}H and ^{13}C NMR spectra were recorded on Bruker AV600 spectrophotometer at 600 and 150 MHz, respectively. Chemical shifts are reported in ppm (δ) relative to TMS. The coupling constants, *J* are reported in Hertz (Hz). High-resolution mass spectrometry (HRMS) spectra were acquired on Q-Tof SYNAPT G2-Si HDMS 8 K (Waters) coupled with an electrospray ionization (ESI) source. All compounds were routinely checked by thin layer chromatography (TLC) using precoated silica gel 60 F_{254}, aluminum foil and the spots were detected under UV light at 254 nm and 365 nm or were revealed spraying with 10 % phosphomolybdic acid (PMA) in ethanol.

Compounds **1**, **2**, **5**, **6**, **11**, **14**, **15**, [5], **7**, **8** [9], **16** [8], **17**, **20**–**22** [7], **23**, **24** [6] were prepared according to literature procedures.

4.2. Synthetic procedures

4.2.1. *N-acetyl-3-(3′-adamantan-1-yl)-4′-hydroxy-[1,1′-biphenyl]-4-yl) acrylamide (**3**)*

To a solution of (*E*)-3-(3′-(adamantan-1-yl)-4′-hydroxy-[1,1′-biphenyl]-4-yl)acrylonitrile [5] (47 mg, 0.13 mmol) in acetic anhydride (0.132 mL) *p*-toluensulfonic acid (16 mg, 0.08 mmol) was added and the resulting mixture was heated at 80 °C for 2 h. The reaction was diluted with H_2O and extracted with AcOEt. The organic phase was dried with Na_2SO_4 and concentrated under reduced pressure. The crude was purified by column chromatography (hexane:ethyl acetate 1:9) to obtain compound **3** in 53 % yield (29 mg, *E*:*Z* = 2.45:1) as a white solid. R_f = 0.67 (hexane:ethyl acetate 7:3). ^{1}H NMR (600 MHz, acetone-d_6) δ: (*E*:*Z* = 70:30) 8.02–7.97 (2H isomer *Z*, m); 7.87–7.82 (2H isomer *Z*, m); 7.81–7.75 (4H isomer *E*, m); 7.71 (1H isomer *Z*, d, *J* = 2.5 Hz); 7.67 (1H isomer *E*, d, *J* = 2.2 Hz); 7.65 (1H isomer *E*, d, *J* = 16.5 Hz); 7.61 (1H isomer *Z*, dd, *J* = 8.4 Hz, 2.5 Hz); 7.58 (1H isomer *E*, dd, *J* = 2.2 Hz, 8.3 Hz); 7.43 (1H isomer *Z*, d, *J* = 12.1 Hz); 7.20–7.14 (2H, isomer *Z* + *E*, m); 6.36 (1H isomer *E*, d, *J* = 16.5 Hz); 5.78 (1H isomer *Z*, d, *J* = 12.1 Hz); 2.42–2.38 (6H isomer *E* + *Z*, m); 2.16–2.10 (18H isomer *E* + *Z*, m); 1.88–1.81 (12H isomer *E* + *Z*, m). HRMS (ESI) (*m/z*): $[M + Na]^+$ Calculated $C_{27}H_{29}NO_3Na$ 438.2045; found: 438.2039.

*4.2.2. (E)-3-(3′-adamantan-1-yl)-4′-hydroxy-[1,1′-biphenyl]-4-yl)-1-(1H-imidazol-1-yl)prop-2-en-1-one (**4**)*

To a solution of adarotene (**1**) [5] (50 mg, 0.13 mmol) in dry DMF (1 mL), CDI (21 mg, 0.13 mmol) was added and the mixture was stirred for 24 h. The reaction was diluted with ethyl acetate, washed with H_2O, dried over anhydrous Na_2SO_4 and concentrated under reduced pressure. The crude was purified by column chromatography (CH_2Cl_2:MeOH 24:1) to afford compound **4** in 20 % yield (11 mg) as a yellow solid. R_f = 0.17 (RP-18 TLC MeOH:H_2O 9:1). ^{1}H NMR (600 MHz, DMSO-d_6) δ: 9.61 (1H, s); 8.78 (1H, s); 8.05 (1H, d, J = 15.4 Hz); 8.00–7.95 (3H, m); 7.74–7.70 (2H, m); 7.68 (1H, d; J = 15.4 Hz); 7.47–7.40 (2H, m); 7.18–7.15 (1H, m); 6.90 (1H, d, J = 8.2 Hz); 2.20–2.21 (6H, m); 2.10–2.20 (3H, m); 1.83–1.69 (6H, m). ^{13}C NMR (150 MHz, DMSO-d_6) δ: 162.1; 156.7; 148.4; 143.8; 137.3; 136.0; 131.8; 130.6; 130.0 (×2C); 129.5; 126.3 (×2C); 125.2; 124.9; 117.0; 116.8; 115.2; 3C missing due to the overlap with solvent signal, 36.6 (×3C); 36.3; 28.4 (×3C). HRMS (ESI) (*m/z*): [M -H]$^-$ Calculated $C_{28}H_{28}N_2O_2$ 423.2073; found: 423.2073.

*4.2.3. 3-(Adamantan-1-yl)-4′-(3-hydroxyprop-1-yn-1-yl)-[1,1′-biphenyl]-4-ol (**9**)*

2-(adamantan-1-yl)-4-(4-bromophenyl)phenol (2 g, 5.22 mmol), was added to a mixture of CuI (0.017 g, 0.089 mmol), $PdCl_2(Ph_3P)_2$ (0.037 g, 0.052 mmol), diisopropylamine (17.4 mL) and TEA (3.48 mL). The resulting mixture was stirred for 30 min at room temperature, added with propargyl alcohol (0.33 g, 5.74 mmol), heated at 60 °C for 20 h. The reaction mixture was diluted with H_2O and ice, acidified with 2 N HCl and extracted with AcOEt. The organic phase was dried over anhydrous Na_2SO_4 and concentrated under reduced pressure. The crude was purified by column chromatography (hexane:ethyl acetate 90:10 → 70:30) to obtain **9** in 19 % yield (347 mg) as a white solid. R_f = 0.67 (hexane:ethyl acetate 7:3). m.p.: 200 °C. ^{1}H NMR (600 MHz, $CDCl_3$) δ: 7.37–7.55 (5H, m); 7.27 (1H, dd, J = 7.8 Hz, J = 2.6 Hz); 6.69 (1H, d, J = 7.8 Hz); 5.40 (1H, d, J = 11.3 Hz); 2.17 (6H, s), 4.50 (1H, s); 1.80 (6H, s), 2.13 (3H, s). ^{13}C NMR (150 MHz, $CDCl_3$) δ: 154.4; 141.6; 136.8; 132.8; 132.0 (×2C); 126.6 (×2C); 126.0; 125.3; 120.5; 117.2; 87.4; 85.8; 51.8; 40.5 (×3C); 37.0 (×3C); 29.0 (×4C). HRMS (ESI) (*m/z*): [M -H]$^-$ Calculated $C_{25}H_{26}O_2$ 357.1855; found: 357.1853.

4.2.4. 3-(4-(7-adamantan-1-yl)benzo[d][1,3]dioxol-5-yl)phenyl)prop-2-yn-1-ol (10)

To a solution of 3-(4-(4,4,5,5-tetramethyl-1,3,2-dioxaborolan-2-yl) phenyl)prop-2-yn-1-ol **29** (50 mg, 0.19 mmol) in dry DMF (1 mL), TBDMSCl (35 mg, 0.23 mmol) and imidazole (26 mg, 0.38 mmol) were added at 0 °C and the resulting mixture was stirred for 2 h at room temperature. The mixture was quenched with H_2O and sat. $NaHCO_3$, extracted with ethyl acetate, dried over anhydrous Na_2SO_4 and concentrated under reduced pressure. The crude was purified by column chromatography (hexane:ethyl acetate 95:5) to afford *tert*-butyldimethyl((3-(4-(4,4,5,5-tetramethyl-1,3,2-dioxaborolan-2-yl)phenyl) prop-2-yn-1-yl)oxy)silane **30** in 51 % yield (36 mg) as a colourless oil. R_f = 0.83 (hexane:ethyl acetate 95:5). ^{1}H NMR (600 MHz, $CDCl_3$) δ: 7.76–7.70 (2H, m); 7.44–7.39 (2H, m); 4.54 (2H, s); 1.33 (12H, s); 0.93 (9H, s); 0.17 (6H, s).

To a solution of compound **30** (60 mg, 0.18 mmol) in dry dioxane (0.5 mL) **31** (35 mg, 0.09 mmol), Na_2CO_3 2 M (0.131 mL) and catalyst $PdCl_2$(dppf)•CH_2Cl_2 (2 mg, 0.003 mmol) were added and the mixture was refluxed for 3 h. The reaction was diluted with AcOEt, washed with H_2O, dried over anhydrous Na_2SO_4 and concentrated under reduced pressure. The crude was purified by column chromatography in hexane to afford ((3-(4-(7-((3*R*,5*R*,7*R*)-adamantan-1-yl)benzo[*d*][1,3]dioxol-5-yl)phenyl)prop-2-yn-1-yl)oxy)(*tert*-butyl)dimethylsilane in 31 % yield (14 mg) as a white solid. R_f = 0.88 (hexane:ethyl acetate 98:2). ^{1}H NMR (600 MHz, $CDCl_3$) δ: 7.47–7.44 (2H, m); 6.96 (1H, d, J = 1.8 Hz); 6.94 (1H, d, J = 1.8 Hz); 6.00–5.96 (2H, m); 4.56 (2H, s); 2.14–2.0 (9H, m); 1.84–1.76 (6H, m); 0.95 (9H, s); 0.18 (6H, s).

To a solution of the above compound (14 mg, 0.027 mmol) in dry THF (0.3 mL) 1 M TBAF in THF (0.054 mL) was added and the resulting mixture was stirred for 30 min at room temperature. The reaction was concentrated under reduced pressure and crude was purified by column chromatography (hexane:ethyl acetate 7:3) to afford product **10** in 30 % yield (4 mg) as a pale-yellow solid. R_f = 0.73 (hexane:ethyl acetate 7:3). ^{1}H NMR (600 MHz, CH_3OH-d_4) δ: 7.56–7.50 (2H, m); 7.49–7.43 (2H, m); 7.04–6.94 (2H, m); 5.99 (2H, s); 4.43 (2H, s); 2.17–2.06 (9H, m); 1.89–1.80 (6H, m). HRMS (ESI) (*m/z*): [M + Na]$^+$ Calculated $C_{26}H_{26}O_3Na$ 409.1780; found: 409.1788.

*4.2.5. 3-(adamantan-1-yl)-4′-(hydroxymethyl)-[1,1′-biphenyl]-4-ol (**12**)*

To a solution of 3′-((3*R*,5*R*,7*R*)-adamantan-1-yl)-4′-hydroxy-[1,1′-biphenyl]-4-carbaldehyde **14** [5] (40 mg, 0.12 mmol) in MeOH (1 mL), $NaBH_4$ (18 mg, 0.48 mmol) was gradually added and the resulting mixture was stirred 30 min at room temperature. The reaction was concentrated under reduced pressure and the residue was treated with water and acidified with 1 M HCl. The resulting precipitate was filtered and purified by column chromatography (hexane:ethyl acetate 7:3) to obtain product **12** in 60 % yield (24 mg) as a white solid. R_f = 0.14 (hexane:ethyl acetate 8:2). ^{1}H NMR (600 MHz, $CDCl_3$) δ: 7.60–7.54 (2H, m); 7.48 (1H, d, J = 2.2 Hz); 7.46–7.42 (2H, m); 7.32 (1H, dd, J = 2.2 Hz, 8.0 Hz); 6.75 (1H, d, J = 8.0 Hz); 4.99 (1H, bs); 4.77 (2H, s); 2.26–2.18 (6H, m); 2.17–2.08 (3H, m); 1.89–1.77 (6H, m). ^{13}C NMR (150 MHz, $CDCl_3$) δ: 154.3; 141.2; 139.1; 136.8; 133.5; 127.6 (×2C); 127.1 (×2C); 126.2; 125.4; 117.3; 65.4; 40.7 (×3C); 37.2 (×3C); 37.0; 29.2 (×3C). HRMS (ESI) (*m/z*): [M -H]$^-$ Calculated $C_{23}H_{26}O_2$ 333.1855; found: 333.1859.

*4.2.6. (3′-(adamantan-1-yl)-4′-hydroxy-[1,1′-biphenyl]-4-yl)boronic acid (**13**)*

To a solution of compound **27** [5] (50 mg, 0.13 mmol) in dry DMF (0.3 mL) KOAc (57 mg, 0.56 mmol), bis(pinacolato)diboron (50 mg, 0.2 mmol) and catalyst $PdCl_2$(dppf)•CH_2Cl_2 (5 mg, 0.007 mmol) were added at room temperature and the mixture was then heated at 80 °C for 6 h. The reaction was concentrated, then diluted with H_2O and extracted with AcOEt. The organic phase was dried over anhydrous Na_2SO_4 and concentrated under reduced pressure. The crude was purified by column chromatography (hexane:ethyl acetate 9:1) to afford 3-((3*R*,5*R*,7*R*)-adamantan-1-yl)-4′-(4,4,5,5-tetramethyl-1,3,2-dioxaborolan-2-yl)-[1,1′-biphenyl]-4-ol in quantitative yield (56 mg) as a dense colourless oil. R_f = 0.57 (hexane:ethyl acetate 8:2). ^{1}H NMR (600 MHz, $(CH_3)_2CO$-d_6) δ: 7.87–7.82 (2H, m); 7.57–7.53 (2H, m); 7.47 (1H, d, J = 2.2 Hz); 7.31 (1H, dd, J = 2.2 Hz, 8.1 Hz); 6.72 (1H, d, J = 8.1 Hz); 2.22–2.15 (6H, m); 2.13–2.08 (3H, m); 1.84–1.74 (6H, m); 1.36 (12H, s).

To a solution of above compound (37 mg, 0.08 mmol) in acetone: H_2O 2:1 (0.6 mL) CH_3COONH_4 (20 mg, 0.26 mmol) and $NaIO_4$ (55 mg, 0.26 mmol) were added and the resulting mixture was stirred for 18 h at room temperature. The reaction was concentrated, then diluted with brine and extracted with ethyl acetate. The organic phase was dried with anhydrous Na_2SO_4 and concentrated under reduced pressure to afford product **13** in 96 % yield (26 mg) as a white solid without further purification. R_f = 0.35 (RP-18 TLC MeOH:H_2O 9:1). ^{1}H NMR (600 MHz, $(CH_3)_2CO$-d_6) δ: 8.47 (1H, bs); 7.97–7.89 (2H, m); 7.65–7.56 (2H, m); 7.53–7.47 (1H, m); 7.42–7.31 (1H, m); 7.19–7.04 (1H, bs); 6.93 (1H, d, J = 8.2 Hz); 2.37–2.18 (6H, m); 2.15–2.10 (3H, m); 1.90–1.70 (6H, m). ^{13}C NMR (150 MHz, $(CH_3)_2CO$-d_6) δ: 156.8; 144.2; 137.3; 135.5 (×2C); 133.0; 126.3 (×2C);126.2; 125.9; 117.8; 117.6; 41.1 (×3C); 37.8 (×3C); 37.6; 3C missing due to the overlapping with solvent signal. HRMS (ESI) (*m/z*): [M -H]$^-$ Calculated $C_{22}H_{25}BO_3$ 346.1855; found: 346.1859.

*4.2.7. (2E)-3-(3′-adamantan-1-yl)-2-(E)-((allyloxy)imino)methyl)-4′-hydroxy-[1,1′-biphenyl]-4-yl)acrylic acid (**18**)*

To a solution of (*E*)-3-(3′-adamantan-1-yl)-4′-((*tert*-butyldimethylsilyl)oxy)-2-formyl-[1,1′-biphenyl]-4-yl)acrylate **32** [5] (40 mg, 0.08 mmol) in EtOH (0.8 mL) *O*-allylhydroxylamine hydrochloride (25 mg, 0.27 mmol) and pyridine (127 mg, 1.6 mmol) were added and the

resulting mixture was refluxed for 4 h. The reaction was concentrated under reduced pressure and purified by column chromatography (hexane:ethyl acetate 95:5) to afford methyl (2*E*)-3-(3′-adamantan-1-yl)-2-(((allyloxy)imino)methyl)-4′-((*tert*-butyldimethylsilyl)oxy)-[1,1′-biphenyl]-4-yl)acrylate in 94 % yield (44 mg) as a white solid. $R_f = 0.74$ (hexane:ethyl acetate 8:2). ^{1}H NMR (600 MHz, $CDCl_3$) δ: 8.17 (1H, s); 8.10 (1H, d, $J = 1.8$ Hz); 7.77 (1H, d, $J = 16.2$ Hz); 7.58 (1H, dd, $J = 1.8$ Hz, 8.2 Hz); 7.40 (1H, d, $J = 8.2$ Hz); 7.19 (1H, d, $J = 2.4$ Hz); 7.04 (1H, dd, $J = 2.4$ Hz, 8.3 Hz); 6.87 (1H, d, $J = 8.3$ Hz); 6.54 (1H, d, $J = 16.2$ Hz); 6.13–6.00 (1H, m); 5.42–5.35 (1H, m); 5.31–5.26 (1H, m); 4.76–4.67 (2H, m); 3.87 (3H, s); 2.20–2.06 (9H, m); 1.87–1.74 (6H, m); 1.10 (9H, s); 0.42 (6H, s).

The above compound (35 mg, 0.06 mmol) was dissolved in 1 M NaOH solution in MeOH (3 mL) and refluxed for 2 h. The reaction was concentrated under reduced pressure, diluted with cold water and acidified with 1 M HCl. The resulting precipitate was filtered, washed with H_2O and dried to afford **18** in 85 % yield (23 mg) as a white solid without further purification. $R_f = 0.46$ (RP-18 TLC MeOH:H_2O 9:1). ^{1}H NMR (600 MHz, $CDCl_3$) δ: 8.16–8.11 (2H, m); 7.85 (1H, d, $J = 16.2$ Hz); 7.61 (1H, dd, $J = 1.7$ Hz, 8.3 Hz); 7.41 (1H, d, $J = 8.3$ Hz); 7.91 (1H, d, $J = 2.2$ Hz); 7.05 (1H, dd, $J = 2.2$ Hz, 8.4 Hz); 6.75 (1H, d, $J = 8.4$ Hz); 6.56 (1H, d, $J = 16.2$ Hz); 6.11–6.00 (1H, m); 5.42–5.35 (1H, m); 5.32–5.23 (1H, m); 4.78–4.67 (2H, m); 2.22–2.07 (9H, m); 1.88–1.74 (6H, m). ^{13}C NMR (150 MHz, $CDCl_3$) δ: 170.4; 154.4; 148.1; 146.3; 144.4; 136.5; 134.0; 132.8; 130.9; 130.8; 130.4; 128.8; 127.8 (×2C); 126.5; 117.9; 117.2; 116.7; 75.2; 40.5 (×3C); 37.0; 36.8 (×3C); 30.0 (×3C). HRMS (ESI) (*m/z*): [M -H]$^-$ Calculated $C_{29}H_{31}NO_4$ 456.2175; found: 456.2175.

*4.2.8. (2E)-3-(3′-adamantan-1-yl)-2-((E)-((benzyloxy)imino)methyl)-4′-hydroxy-[1,1′-biphenyl]-4-yl)acrylic acid (**19**)*

To a solution of (*E*)-3-(3′-adamantan-1-yl)-4′-((*tert*-butyldimethylsilyl)oxy)-2-formyl-[1,1′-biphenyl]-4-yl)acrylate **32** [5] (50 mg, 0.09 mmol) in EtOH (1 mL), *O*-benzylhydroxylamine hydrochloride (45 mg, 0.28 mmol) and pyridine (142 mg, 1.8 mmol) were added and the resulting mixture was heated at reflux for 4 h. The reaction was concentrated under reduced pressure and the crude was purified by column chromatography (hexane:ethyl acetate 95:5) to afford product methyl (2*E*)-3-(3′-adamantan-1-yl)-2-(((benzyloxy)imino)methyl)-4′-((*tert*-butyldimethylsilyl)oxy)-[1,1′-biphenyl]-4-yl)acrylate in 56 % yield (32 mg) as a pale-yellow solid. $R_f = 0.72$ (hexane:ethyl acetate = 8:2). ^{1}H NMR (600 MHz, $CDCl_3$) δ: 8.20 (1H, s); 8.11 (1H, d, $J = 1.8$ Hz); 7.77 (1H, d, $J = 16.2$ Hz); 7.58 (1H, dd, $J = 1.8$ Hz, 8.1 Hz); 7.50–7.32 (6H, m); 7.17 (1H, d, $J = 2.0$ Hz); 7.01 (1H, dd, $J = 2.0$ Hz, 8.1 Hz); 6.85 (1H, d, $J = 81$ Hz); 6,54 (1H, d, $J = 16.2$ Hz); 5.25 (2H, s); 3.86 (3H, s); 2.21–2.05 (9H, m); 1.87–1.74 (6H, m); 1.10 (9H, s); 0.40 (6H, s).

The above compound (30 mg, 0.05 mmol) was dissolved in 1 M NaOH solution in MeOH (2.5 mL) and refluxed for 3 h. The reaction was concentrated under reduced pressure, diluted with cold water and acidified with HCl 1 M. The resulting precipitate was filtered, washed with H_2O and dried to afford **19** in quantitative yield (27 mg) as a pale-yellow solid without further purification. $R_f = 0.42$ (RP-18 TLC MeOH:H_2O = 9:1). ^{1}H NMR (600 MHz, $CDCl_3$) δ: 8.17 (1H, s); 8.13 (1H, d, $J = 1.7$ Hz); 7.86 (1H, d, $J = 15.8$ Hz); 7.61 (1H, dd, $J = 1.7$ Hz, 7.9 Hz); 7.47–7.43 (2H, m); 7.42–7.38 (3H, m); 7.37–7.33 (1H, m); 7.17 (1H, d, $J = 2.2$ Hz); 7.03 (1H, dd, $J = 2.2$ Hz, 8.1 Hz); 6.73 (1H, d, $J = 8.1$ Hz); 6.56 (1H, d, $J = 15.8$ Hz); 5.26 (2H, s); 2.19–2.08 (9H, m); 1.85–1.77 (6H, m). ^{13}C NMR (150 MHz, $CDCl_3$) δ: 171.5; 154.6; 148.4; 146.5; 144.7; 137.6; 136.7; 132.9; 131.0 (×2C); 130.5; 129.0; 128.9; 128.6.4 (×2C); 128.5 (×2C); 128.1; 128.0; 126.8; 117.6; 116.9; 76.6; 40.7 (×3C); 37.1 (×3C); 37.0; 29.1 (×3C). HRMS (ESI) (*m/z*): [M -H]$^-$ Calculated $C_{33}H_{33}NO_4$ 506.2331; found: 506.2328.

*4.2.9. (E)-3-(3′-((3R,5R,7R)-adamantan-1-yl)-5′-((E)-(tert-butoxyimino)methyl)-4′-hydroxy-[1,1′-biphenyl]-4-yl)acrylic acid (**25**)*

To a solution of 5-(adamantan-1-yl)-4′-bromo-4-hydroxy-[1,1′-biphenyl]-3-carbaldehyde **28** [9] (200 mg, 0.48 mmol), $Pd(OAc)_2$ (1 mg, 0.005 mmol) and tri(*o*-tolyl)phosphine (6 mg, 0.019 mmol) in Et_3N (0.5 mL) *tert*-butyl acrylate (100 mg, 0.78 mmol) was added and the resulting mixture was heated at 110 °C for 4 h. The reaction was diluted with cold water, acidified with 1 M HCl and extracted with ethyl acetate. The organic phase was dried with anhydrous Na_2SO_4 and concentrated under reduced pressure. The residue was crystallized from Et_2O:hexane 1:9 to obtain *tert*-butyl (*E*)-3-(3′-(adamantan-1-yl)-5′-formyl-4′-hydroxy-[1,1′-biphenyl]-4-yl) acrylate in 60 % yield (131 mg) as a yellow solid. $R_f = 0.79$ (hexane:ethyl acetate 8:2). ^{1}H NMR (600 MHz, $CDCl_3$) δ: 11.90 (1H, s); 9.99 (1H, s); 7.75 (1H, d, $J = 2.2$ Hz); 7.65 (1H, d, $J = 15.7$ Hz); 7.64 (1H, d, $J = 2.2$ Hz); 7.63–7.58 (4H, m); 6.44 (1H, d, $J = 15.7$ Hz); 2.26–2.17 (6H, m); 2.16–2.10 (3H, m); 1.90–1.80 (6H, m); 1.58 (9H, s).

To a solution of the above compound (50 mg, 0.1 mmol) in EtOH (1 mL) *O*-allylhydroxylamine hydrochloride (41 mg, 0.3 mmol) and pyridine (158 mg, 2 mmol) were added and the resulting mixture was refluxed for 2 h. The reaction was concentrated under reduced pressure and purified by column chromatography (hexane:ethyl acetate 95:5) to *tert*-butyl (2*E*)-3-(3′-((3*R*,5*R*,7*R*)-adamantan-1-yl)-5′-((*tert*-butoxyimino) methyl)-4′-hydroxy-[1,1′-biphenyl]-4-yl)acrylate in quantitative yield (53 mg) as a white solid. $R_f = 0.80$ (hexane:ethyl acetate 8:2). ^{1}H NMR (600 MHz, $CDCl_3$) δ: 10.71 (1H, s); 8.26 (1H, s); 7.74 (1H, d, $J = 16.2$ Hz); 7.51 (1H, d, $J = 2.0$ Hz); 7.26 (1H, d, $J = 2.0$ Hz); 6.42 (1H, d, $J = 16.2$ Hz); 2.30–2.20 (6H, m); 2.18–2.11 (3H, m); 1.92–1.77 (6H, m); 1.58 (9H, s); 1.45 (9H, s).

To a solution of the above compound (50 mg, 0.09 mmol) in dry CH_2Cl_2 (1.7 mL) TFA (0.75 mL) was added at 0 °C and the resulting mixture was stirred at 0 °C for 2 h. The reaction was concentrated under reduced pressure. After azeotropic removal of TFA with toluene, the residue was crystallized from Et_2O to obtain product **25** in 95 % yield (41 mg) as a white solid. $R_f = 0.18$ (RP-18 TLC MeOH: H_2O 9:1). ^{1}H NMR (600 MHz, $CDCl_3$) δ: 10.71 (1H, s); 8.24 (1H, s); 7.81 (1H, d, $J = 16.0$ Hz); 7.66–7.54 (4H, m); 7.51–7.47 (1H, m); 7.26–7.23 (1H, m); 6.47 (1H, d, $J = 16.0$ Hz); 2.28–2.16 (6H, m); 2.15–2.06 (3H, m); 1.90–1.76 (6H, m); 1.42 (9H, s). ^{13}C NMR (150 MHz, $CDCl_3$) δ: 171.6; 157.0; 151.3; 146.7; 143.4; 138.0; 132.3; 130.8; 129.0; 128.9 (×2C); 128.2; 127.1 (×2C); 117.6; 116.4; 79.9; 40.2 (×3C); 37.3; 37.1 (×3C); 20.1 (×3C); 27.4 (×3C). HRMS (ESI) (*m/z*): [M -H]$^-$ Calculated $C_{33}H_{35}NO_4$ 472.2488; found: 472.2487.

*4.2.10. 3-(3′-(adamantan-1-yl)-2-((E)-(tert-butoxyimino)methyl)-4′-hydroxy-[1,1′-biphenyl]-4-yl)propiolic acid (**26**)*

To solution of compound **32** (135 mg, 0.25 mmol) [5] in CH_2Cl_2 (2.5 mL) at 0 °C, pyridinium bromide (118 mg, 0.33 mmol) was added. The reaction was stirred 4 days at rt. The mixture was diluted in CH_2Cl_2, washed with 5 % aq $Na_2S_2O_3$ and dried over anhydrous Na_2SO_4. The crude was purified by flash chromatography in hexane:ethyl acetate 24:1 to give 140 mg of compound **37** (79 %). m.p. 193.9 °C. ^{1}H NMR (600 MHz, $CDCl_3$) δ: 10.02 (1H, s); 8.024 (1H, d, $J = 1.8$ Hz); 7.62 (1H, dd, $J = 1.8$ Hz, 7.8 Hz); 7.49 (1H, d, $J = 7.8$ Hz); 7.21 (1H, d, $J = 2.2$ Hz); 7.09 (1H, dd, $J = 2.2$ Hz, 8.1 Hz); 6.89 (1H, d, $J = 8.1$ Hz); 5.43 (1H, d, $J = 11.7$ Hz); 4.89 (1H, d, $J = 11.7$ Hz); 3.93 (3H, s); 2.16–2.05 (9H, m); 1.82–1.71 (m, 6H); 1.07 (s, 9H); 0.40 (s, 6H).

A solution of 106 mg (0.15 mmol) of **33** in 3 mL of ethanol is added with 246 μL of pyridine and 57 mg (0.45 mmol) of *O*-*tert*-butylhydroxylamine hydrochloride and refluxed 2 h. Filtration, and drying gave 74 mg (65 %) of methyl (*E*)-3-(3′-(adamantan-1-yl)-2-((*tert*-butoxyimino) methyl)-4′-((*tert*-butyldimethylsilyl)oxy)-[1,1′-biphenyl]-4-yl)-2,3-dibromopropanoate as a white solid. m.p. 170.1 °C. ^{1}H NMR (600 MHz, $CDCl_3$) δ: 8.04 (1H, s); 7.94 (1H, d, $J = 1.7$ Hz); 7.40 (1H, dd, $J = 1.7$ Hz, 8.2 Hz); 7.35 (1H, d, $J = 8.2$ Hz); 7.15 (1H, d, $J = 2.2$ Hz); 7.01 (1H, dd, $J = 2.2$ Hz, 8.2 Hz); 6.82 (1H, d, $J = 8.2$ Hz); 5.43 (1H, d, $J = 11.7$ Hz); 4.91 (1H, d, $J = 11.7$ Hz); 3.91 (3H, s); 2.15–2.03 (9H, m); 1.82–1.73 (m, 6H); 1.36 (s, 9H); 1.07 (s, 9H); 0.38 (s, 6H).

To a solution of the above compound (190 mg, 0.03 mmol) in 2-propanol (1.3 mL), KOH (14 mg, 0.21 mmol) was added and the mixture

refluxed for 12 h. After evaporation, taking up with water, addition of 1 N HCl to acid pH, filtration, and drying, the crude was triturated in Et_2O. The resulting precipitate (28 mg) was purified by preparative chromatography on TLC RP-18 in CH_3OH: H_2O 8:2 to give 38 mg of compound **26** (30 %). ^{1}H NMR (600 MHz, DMSO-d_6,) δ: 9.75 (1H, s); 7.90 (1H, s); 7.74 (1H, d, $J = 1.2$ Hz); 7.44 (1H, dd, $J = 12.$ Hz, $J = 7.7$ Hz); 7.35 (1H, d, $J = 7.7$ Hz); 7.04 (1H, dd, $J = 1.8$ Hz, $J = 8.4$ Hz); 6.98 (1H, d, $J = 1.8$ Hz); 6.90 (1H, d, $J = 8.4$ Hz); 2.18–2.00 (9H, m); 1.81–1.67 (6H, m), 1.31 (9H, s). ^{13}C NMR (150 MHz, DMSO-d_6) δ: 156.1; 155.3; 146.2; 145.6; 141.2; 135.2; 132.0; 130.1; 128.9; 128.4; 128.0; 127.2; 121.6; 92.3; 78.6; 75.8; 3C missing due to the overlapping with solvent signal; 36.6 (×3C); 36.2; 28.4 (×3C); 27.4 (×3C). HRMS (ESI) (*m/z*): $[M-H]^-$ Calculated $C_{30}H_{33}NO_4$ 470.2331; found: 470.2324.

4.3. Antimicrobial activity

The minimum inhibitory concentrations of the tested compounds were determined by the broth microdilution assays in 96-multiwell plates, as previously reported with some modifications [33]. These strains were from the American Type Culture Collection (ATCC): *E. coli* ATCC 25922, *S. aureus* ATCC 25923, *S. epidermidis* ATCC 12228 and *S. aureus* ATCC 43300. The MDR *S. aureus* #2, *S. aureus* 13667073 and *S. aureus* 02216108 clinical isolates were from the strain collection of Policlinico Umberto I (Sapienza, University of Rome). Bacteria were grown in Luria-Bertani (LB) broth at 37 °C with gentle shaking until an optical density (O.D.) of 0.8 was reached (λ = 590 nm). Compounds were serially two-fold diluted in 50 μL cation-adjusted Mueller Hinton II Broth (MH^+) and aliquots (50 μL) of bacterial cells were added to each well to reach a final concentration of $5x10^5$ colony forming unit (CFU)/mL. The plates were then incubated at 37 °C with gentle shaking and the absence/presence of microbial growth was visually observed after 24 h of incubation.

4.4. Membrane permeabilization: SYTOX green assay

S. aureus ATCC 25923 was chosen as reference strain, and it was grown as previously described. The assay was conducted as previously described, with some modifications [34]. When an OD of 0.8 was reached, the bacterial culture was centrifuged for 10 min at 1400 × g, washed in buffer A (5 mM Hepes, 110 mM KCl, 15 mM D-glucose, pH 7.3) and resuspended in buffer A at an OD of 0.8. Approximately $1x10^7$ cfu/mL were incubated with 1 μM of SYTOX Green (Invitrogen™, Thermo Fisher Scientific Inc.) in buffer A for 5 min in the darkness. After compound addition (time = 0), changes in fluorescence intensity (λ_{exc} = 485 nm, λ_{ems} = 535 nm) caused by the binding of the dye to intracellular DNA were monitored for 30 min in a microplate reader (Infinite M200, Tecan, Salzburg, Austria) at 37 °C. After the kinetics, aliquots were diluted and spread onto LB agar plates for CFU counting and bacterial death determination. Controls were cells treated with the vehicle.

4.5. Combination with rifaximin

The capability of compound **17** to potentiate the inhibitory effect of RIF against *S. aureus* ATCC 25923 and *S. aureus* #2 MDR strains was monitored in the microplate reader (Infinite M200) at 37 °C, as previously reported with some modifications [35]. Bacteria were grown as previously reported and diluted to reach a final concentration of $5x10^5$ CFU/mL in MH^+. The cells were treated with compound **17** at its 1/2 MIC (i.e., 2 μM), ½ MIC of RIF and their combination. Microbial growth was monitored by recording the absorbance of each well for 16 h.

4.6. Animal studies

CD1 Mice female 4–6 weeks old, were purchased from Charles River Laboratories (Calco, Lecco) Italy) and kept in Polysulfone IVC cages (33.2 × 15 × 13 cm, Tecniplast) with 75 complete changes of filtered air per hour (HEPA H 14 filter); autoclaved dust-free bedding and mouse house enrichment device (Tecniplast) were used.

All animal studies were conducted in accordance with ethics approval obtained from the Italian Ministry of Health and all experiments were in accordance with the European guidelines for the care and use of laboratory animals. All procedures were performed under deep isoflurane anesthesia and at the end of experiments were sacrificed by cervical dislocation.

Table 5
Lipid composition of the *S. aureus* model bilayers. The two leaflets of each bilayer have identical lipid composition. The fatty acyl tails of the *S. aureus* phospholipids were all 16 carbon anteiso-branched chains.

Phospholipid head groups	CHARMM-GUI name	Number in each layer
phosphatidylglycerol (PG)	DPPG (16:0/16:0)	54
Cardiolipin (CL)	PMCL2 (16:0/16:0)	5
lysyl-phosphatidylglycerol (Lys-PG)	DPPGK (16:0/16:0)	36

4.7. Pharmacokinetic studies

For pharmacokinetic analysis, 16 CD1 mice per dose (50, 100, and 150 mg/kg) were recruited. In order to collect plasma from 4 animals/group (approximately 100 μL/mouse) at each time point (0.25, 0.50, 1, 2, 4, 7, and 24 h), blood from each group was sampled twice at time intervals of at least 2 h between the first and second sampling. Blood was collected into sodium-heparinized test tubes, centrifuged (5 min, 6000g at 4 °C) and the resultant plasma stored at − 20 °C until analysis.

The developed quantitative method for PK analysis utilized reverse-phase high-performance liquid chromatography (HPLC) with the following equipment: HPLC system (Waters 2695-PDA 2998) equipped with a Zorbax Eclipse XDB-C18 column. The stationary phase used was a C18 column, while the mobile phase was an isocratic solution of 0.1 % formic acid and 70 % acetonitrile in water. The analysis duration was 5 min, during which AB473 eluted at 2.4 min, while the internal standard (Adarotene) eluted at approximately 3.9 min.

Detection was performed using fluorimetric detection, with excitation at 330 nm and emission at 475 nm.

4.8. Simulation systems

A symmetric pure lipid bilayer membrane systems of *S. aureus* was built using the CHARMM-GUI Membrane Builder tool [11,12]. The phospholipid composition of the *S. aureus* lipid bilayer in the simulations was 56.8 % phosphatidylglycerol (PG), 37.9 % Lys-PG, and 5.3 % diphosphatidylglycerol (DPG; also referred as Cardiolipin (CL)) which mimics the phospholipid composition of *S. aureus* membrane (Table 5), following a protocol adapted from previous MD studies of membrane-containing systems [10,13].

A pure lipid bilayer system was built to study the stability of the membrane. A total of 95 lipid molecules were placed in each lipid bilayer with its center at z = 0. A water layer of 50 Å thickness was added above and below the lipid bilayer for the systems. The system was neutralized with Na^+ and Cl^- ions with a concentration of 0.145 M according with the parameters of CHARMM-GUI. Then, the Multicomponent Assembler tool was used to build the systems with the different small molecules placed randomly in the solvent area. Ligands **9**, **10**, **17** as well as the reference compound **CD437** [10] retrieved from the literature were drawn on the sketchpad powered by Marvin JS [11] and were parametrized using the standard CHARMM FF parameters of the CHARMM-GUI ligand reader and modeler tool [36]. The membrane systems with the small molecules were then parametrized using a membrane thickness of 50 Å and the box XY length of 79.50 Å, solvated with a 50 Å water layer on both sides with at least 50 water molecules

Table 6
Simulation details of the equilibrium simulations.

Compound	Solvent	ions	Simulation length
–	11,928 H_2O	Na^+ 82; Cl^- 26	1 replica × 500 ns
CD437	18,861 H_2O	Na^+ 107; Cl^- 50	1 replica × 500 ns
9	18,813 H_2O	Na^+106; Cl^- 50	2 replicas × 500 ns
10	18,855 H_2O	Na^+ 106; Cl^- 50	2 replicas × 500 ns
2 × 9	18,784 H_2O	Na^+ 106; Cl^- 50	1 replica × 500 ns
17(*E*)	18,837 H_2O	Na^+ 106; Cl^- 49	1 replica × 500 ns
17(*Z*)	18,800 H_2O	Na^+ 106; Cl^- 49	1 replica × 500 ns

per lipid. All systems were neutralized with Na^+ and Cl^- ions with a concentration of 0.145 M according with the parameters of CHARMM-GUI. All-atom MD simulations were performed using the CHARMM36m38 force field [37,38]. Once the systems were built with CHARMM-GUI, the topology and coordinate files were obtained for AMBER [39,40].

4.9. Molecular dynamics simulations

The interaction between **9**, **10**, **17(*E*)**, **17(*Z*)**, and the reference control **CD437** with the *S. aureus* membrane model was investigated by MD simulations with AMBER18 [16,17]. The initial systems were first energy minimized for 25.000 steps. The first 1500 steps utilized the steepest descent algorithm before shifting to the conjugate gradient algorithm for the remaining steps. No positional restraints were applied. The non-bonded cut-off was 12.0 Å. Each system was then heated gradually from 0 to 300 K over 900 ps at constant volume using the Langevin thermostat with a collision frequency set to 2 ps^{-1}. Then, the system was maintained at 300 K over 100 ps. Box density was equilibrated at constant pressure and constant temperature (300 K) over 1 ns using the Berendsen barostat (see Table 6).

Following density equilibration, a preliminary 50 ns MD was run at a constant pressure. Finally, MD trajectories were produced for 500 ns. All systems were run using PME electrostatics in the MD studies. MD trajectories were analysed with CPPTRAJ [41] from the AmberTools package to calculate the root the mass densities along the z-axis and the root-mean-square deviations (RMSD). The study of the interactions after the Md were done with the visualization programme of PyMol [42] or VMD [17].

CRediT authorship contribution statement

Salvatore Princiotto: Writing – original draft, Writing – review & editing, Investigation, Formal analysis, Conceptualization. **Bruno Cassciaro:** Writing – original draft, Writing – review & editing, Investigation, Formal Analysis, Conceptualization. **Alvaro G. Temprano:** Writing – original draft, Writing – review & editing, Investigation, Formal analysis, Conceptualization. **Loana Musso:** Writing – review & editing, Writing – original draft, Methodology, Conceptualization. **Francesca Sacchi:** Investigation. **Maria Rosa Loffredo:** Investigation, Methodology, Conceptualization, Formal analysis. **Floriana Cappiello:** Investigation, Formal analysis. **Federica Sacco:** Validation, Resources. **Giammarco Raponi:** Validation, Resources. **Virginia Perez Fernandez:** Investigation. **Teresa Iucci:** Investigation. **Maria Luisa Mangoni:** Writing – original draft, Writing – review & editing, Supervision, Resources, Conceptualization. **Mattia Mori:** Writing – review & editing, Writing – original draft, Supervision, Resources, Conceptualization. **Sabrina Dallavalle:** Writing – review & editing, Writing – original draft, Supervision, Resources, Conceptualization. **Claudio Pisano:** Writing – review & editing, Writing – original draft, Supervision, Resources, Conceptualization.

Declaration of competing interest

The authors declare that they have no known competing financial interests or personal relationships that could have appeared to influence the work reported in this paper.

Data availability

Data will be made available on request.

Acknowledgments

A.G.T. acknowledges support from the Margarita Salas postdoctoral grant financed by NextGenerationEU European Funds. This article is based upon work from COST Action EURESTOP, CA21145, supported by COST (European Cooperation in Science and Technology). MM acknowledges the partial support by EU funding within the NextGenerationEU-MUR PNRR Extended Partnership initiative on EmergingInfectious Diseases (Project no. PE00000007, INF-ACT). The manuscript was partially funded by Sapienza University of Rome (RM12117A5D5A92A4). Mass spectrometry analyses were performed at the Mass Spectrometry facility of the Unitech COSPECT at the University of Milan (Italy).

Appendix A. Supplementary data

Supplementary data to this article can be found online at https://doi.org/10.1016/j.bioorg.2024.107227.

References

[1] G. Mancuso, A. Midiri, E. Gerace, C. Biondo, Bacterial antibiotic resistance: the most critical pathogens, Pathogens 10 (2021) 1310, https://doi.org/10.3390/pathogens10101310.
[2] J. Ali, Q.A. Rafiq, E. Ratcliffe, Antimicrobial resistance mechanisms and potential synthetic treatments, Future Sci OA 4 (2018) FSO290. https://doi.org/10.4155/fsoa-2017-0109.
[3] F. Ruggieri, N. Compagne, K. Antraygues, M. Eveque, M. Flipo, N. Willand, Antibiotics with novel mode of action as new weapons to fight antimicrobial resistance, Eur. J. Med. Chem. 256 (2023) 115413, https://doi.org/10.1016/j.ejmech.2023.115413.
[4] S. Princiotto, S. Mazzini, L. Musso, F. Arena, S. Dallavalle, C. Pisano, New antimicrobials based on the adarotene scaffold with activity against multi-drug resistant staphylococcus aureus and vancomycin-resistant enterococcus, Antibiotics 10 (2021) 126, https://doi.org/10.3390/antibiotics10020126.
[5] R. Cincinelli, S. Dallavalle, R. Nannei, S. Carella, D. De Zani, L. Merlini, S. Penco, E. Garattini, G. Giannini, C. Pisano, L. Vesci, P. Carminati, V. Zuco, C. Zanchi, F. Zunino, Synthesis and structure–activity relationships of a new series of retinoid-related biphenyl-4-ylacrylic acids endowed with antiproliferative and proapoptotic activity, J. Med. Chem. 48 (2005) 4931–4946, https://doi.org/10.1021/jm049440h.
[6] Z. Xia, R.G. Correa, J.K. Das, L. Farhana, D.J. Castro, J. Yu, R.G. Oshima, J. A. Fontana, J.C. Reed, M.I. Dawson, Analogues of orphan nuclear receptor small heterodimer partner ligand and apoptosis inducer (E)-4-[3-(1-Adamantyl)-4-hydroxyphenyl]-3-chlorocinnamic acid. 2. Impact of 3-chloro group replacement on inhibition of proliferation and induction of apoptosis of, J. Med. Chem. 55 (2012) 233–249, https://doi.org/10.1021/jm2011436.
[7] R. Cincinelli, L. Musso, M.B. Guglielmi, I. La Porta, A. Fucci, E. Luca D'Andrea, F. Cardile, F. Colelli, G. Signorino, N. Darwiche, S. Gervasoni, G. Vistoli, C. Pisano, S. Dallavalle, Novel adamantyl retinoid-related molecules with POLA1 inhibitory activity, Bioorg Chem 104 (2020) 104253, https://doi.org/10.1016/j.bioorg.2020.104253.
[8] L. Musso, R. Cincinelli, V. Zuco, F. Zunino, A. Nurisso, M. Cuendet, G. Giannini, L. Vesci, C. Pisano, S. Dallavalle, Investigation on the ZBG-functionality of phenyl-4-yl-acrylohydroxamic acid derivatives as histone deacetylase inhibitors, Bioorg. Med. Chem. Lett. 25 (2015) 4457–4460, https://doi.org/10.1016/j.bmcl.2015.09.006.
[9] R. Cincinelli, S. Dallavalle, R. Nannei, L. Merlini, S. Penco, G. Giannini, C. Pisano, L. Vesci, F.F. Ferrara, V. Zuco, C. Zanchi, F. Zunino, Synthesis and structure–activity relationships of new antiproliferative and proapoptotic retinoid-related biphenyl-4-yl-acrylic acids, Bioorg. Med. Chem. 15 (2007) 4863–4875, https://doi.org/10.1016/j.bmc.2007.04.057.
[10] W. Kim, W. Zhu, G.L. Hendricks, D. Van Tyne, A.D. Steele, C.E. Keohane, N. Fricke, A.L. Conery, S. Shen, W. Pan, K. Lee, R. Rajamuthiah, B.B. Fuchs, P.M. Vlahovska, W.M. Wuest, M.S. Gilmore, H. Gao, F.M. Ausubel, E. Mylonakis, A new class of synthetic retinoid antibiotics effective against bacterial persisters, Nature 556 (2018) 103–107, https://doi.org/10.1038/nature26157.
[11] S. Jo, T. Kim, V.G. Iyer, W. Im, CHARMM-GUI: A web-based graphical user interface for CHARMM, J. Comput. Chem. 29 (2008) 1859–1865, https://doi.org/10.1002/jcc.20945.

[12] Y. Li, J. Liu, J.C. Gumbart, Preparing Membrane Proteins for Simulation Using CHARMM-GUI BT - Structure and Function of Membrane Proteins, in: I. Schmidt-Krey, J.C. Gumbart (Eds.), Springer US, New York, NY, 2021: pp. 237–251. https://doi.org/10.1007/978-1-0716-1394-8_13.
[13] T.J. Piggot, D.A. Holdbrook, S. Khalid, Electroporation of the E. coli and S. aureus membranes: molecular dynamics simulations of complex bacterial membranes, J. Phys. Chem. B 115 (2011) 13381–13388, https://doi.org/10.1021/jp207013v.
[14] S. Witzke, M. Petersen, T.S. Carpenter, S. Khalid, Molecular dynamics simulations reveal the conformational flexibility of lipid II and its loose association with the defensin plectasin in the staphylococcus aureus membrane, Biochemistry 55 (2016) 3303–3314, https://doi.org/10.1021/acs.biochem.5b01315.
[15] F. Joodaki, L.M. Martin, M.L. Greenfield, Generation and computational characterization of a complex staphylococcus aureus lipid bilayer, Langmuir 38 (2022) 9481–9499, https://doi.org/10.1021/acs.langmuir.2c00483.
[16] D. Case, I. Ben-Shalom, S.R. Brozell, D.S. Cerutti, T. Cheatham, V.W.D. Cruzeiro, T. Darden, R. Duke, D. Ghoreishi, M. Gilson, H. Gohlke, A. Götz, D. Greene, R. Harris, N. Homeyer, Y. Huang, S. Izadi, A. Kovalenko, T. Kurtzman, P. A. Kollman, Amber (2018) 2018.
[17] R. Salomon-Ferrer, D.A. Case, R.C. Walker, An overview of the Amber biomolecular simulation package, WIREs Computational Molecular Science 3 (2013) 198–210, https://doi.org/10.1002/wcms.1121.
[18] J.L. Hofstra, B.R. Grassbaugh, Q.M. Tran, N.R. Armada, H.J.P. de Lijser, Catalytic oxidative cyclization of 2′-arylbenzaldehyde oxime ethers under photoinduced electron transfer conditions, J. Org. Chem. 80 (2015) 256–265, https://doi.org/10.1021/jo502324z.
[19] S. Dallavalle, A. Ferrari, B. Biasotti, L. Merlini, S. Penco, G. Gallo, M. Marzi, M. O. Tinti, R. Martinelli, C. Pisano, P. Carminati, N. Carenini, G. Beretta, P. Perego, M. De Cesare, G. Pratesi, F. Zunino, Novel 7-oxyiminomethyl derivatives of camptothecin with potent in vitro and in vivo antitumor activity, J. Med. Chem. 44 (2001) 3264–3274, https://doi.org/10.1021/jm0108092.
[20] B.S. Pilgrim, A.E. Gatland, C.H.A. Esteves, C.T. McTernan, G.R. Jones, M.R. Tatton, P.A. Procopiou, T.J. Donohoe, Palladium-catalyzed enolate arylation as a key C-C bond-forming reaction for the synthesis of isoquinolines, Org. Biomol. Chem. 14 (2016) 1065–1090, https://doi.org/10.1039/C5OB02320C.
[21] R. Álvarez, B. Vaz, H. Gronemeyer, Á.R. de Lera, Functions, therapeutic applications, and synthesis of retinoids and carotenoids, Chem. Rev. 114 (2014) 1–125, https://doi.org/10.1021/cr400126u.
[22] N. Skrzypczak, P. Przybylski, Modifications, biological origin and antibacterial activity of naphthalenoid ansamycins, Nat. Prod. Rep. 39 (2022) 1653–1677, https://doi.org/10.1039/D2NP00002D.
[23] A. Mariana, K.M. J., G.-Q.K. E., O.D. R., O.C. P., B.D. J., A.M. P., P. Robin, In Vitro Activity of Rifampin, Rifabutin, Rifapentine, and Rifaximin against Planktonic and Biofilm States of Staphylococci Isolated from Periprosthetic Joint Infection, Antimicrob Agents Chemother 63 (2019) 10.1128/aac.00959-19. https://doi.org/10.1128/aac.00959-19.
[24] F. Calanni, C. Renzulli, M. Barbanti, G.C. Viscomi, Rifaximin: beyond the traditional antibiotic activity, J. Antibiot. (Tokyo) 67 (2014) 667–670, https://doi.org/10.1038/ja.2014.106.
[25] A. Rivkin, S. Gim, Rifaximin: new therapeutic indication and future directions, Clin. Ther. 33 (2011) 812–827. https://doi.org/10.1016/j.clinthera.2011.06.007.
[26] S.J. M., R. Joaquin, N.M. M., V. Martha, G. Joaquim, V. Jordi, In Vitro Activity of Rifaximin against Enteropathogens Producing Traveler's Diarrhea, Antimicrob Agents Chemother 45 (2001) 643–644. https://doi.org/10.1128/aac.45.2.643-644.2001.
[27] H.L. DuPont, Z.-D. Jiang, C.D. Ericsson, J.A. Adachi, J.J. Mathewson, M. W. DuPont, E. Palazzini, L.M. Riopel, D. Ashley, F.M. Sandoval, RifaXIMIN VERSUS CIPROFLOXACIN FOR THE TREATMENT of traveler's diarrhea: A randomized, double-blind clinical trial, Clin. Infect. Dis. 33 (2001) 1807–1815, https://doi.org/10.1086/323814.
[28] C. Scarpignato, I. Pelosini, Rifaximin, a poorly absorbed antibiotic: pharmacology and clinical potential, Chemotherapy 51 (2005) 36–66, https://doi.org/10.1159/000081990.
[29] E. Padilla, L. Oms, E. Espejo, L. Gómez, L. Pagespetit, N. Boada, F. Bella, J. Pérez, Rifampin resistance in staphylococci after rifaximin intake for surgical prophylaxis in elective colorectal surgery, Antimicrob. Agents Chemother. 62 (2018), 10.1128/aac.01353-18. https://doi.org/10.1128/AAC.01353-18.
[30] J.W. Betts, L.M. Phee, D.W. Wareham, Rifaximin combined with polymyxins: A potential regimen for selective decontamination of multidrug-resistant bacteria in the digestive tract? J Glob Antimicrob Resist 4 (2016) 11–15. https://doi.org/10.1016/j.jgar.2015.11.008.
[31] J. Fu, Y. Gao, L. Shi, Combination therapy with rifaximin and lactulose in hepatic encephalopathy: A systematic review and meta-analysis, PLoS One 17 (2022) e0267647.
[32] D. Buldain, L. Gortari Castillo, A.V. Buchamer, F. Aliverti, A. Bandoni, L. Marchetti, N. Mestorino, Melaleuca armillaris Essential Oil in Combination With Rifaximin Against Staphylococcus aureus Isolated of Dairy Cows , Frontiers in Veterinary Science 7 (2020). https://www.frontiersin.org/articles/10.3389/fvets.2020.00344.
[33] M.R. Loffredo, F. Savini, S. Bobone, B. Casciaro, H. Franzyk, M.L. Mangoni, L. Stella, Inoculum effect of antimicrobial peptides, Proceedings of the National Academy of Sciences 118 (2021) e2014364118. https://doi.org/10.1073/pnas.2014364118.
[34] B. Casciaro, M.R. Loffredo, F. Cappiello, N. O'Sullivan, C. Tortora, R. Manzer, S. Karmakar, A. Haskell, S.K. Hasan, M.L. Mangoni, KDEON WK-11: A short antipseudomonal peptide with promising potential, Front. Chem. 10 (2022), https://doi.org/10.3389/fchem.2022.1000765.
[35] F. Sacco, C. Bitossi, B. Casciaro, M.R. Loffredo, G. Fabiano, L. Torrini, F. Raponi, G. Raponi, M.L. Mangoni, The antimicrobial peptide Esc(1–21) synergizes with colistin in inhibiting the growth and in killing multidrug resistant acinetobacter baumannii strains, Antibiotics 11 (2022) 234, https://doi.org/10.3390/antibiotics11020234.
[36] S. Kim, J. Lee, S. Jo, C.L. Brooks III, H.S. Lee, W. Im, CHARMM-GUI ligand reader and modeler for CHARMM force field generation of small molecules, J. Comput. Chem. 38 (2017) 1879–1886. https://doi.org/10.1002/jcc.24829.
[37] J. Lee, M. Hitzenberger, M. Rieger, N.R. Kern, M. Zacharias, W. Im, CHARMM-GUI supports the Amber force fields, J. Chem. Phys. 153 (2020) 35103, https://doi.org/10.1063/5.0012280.
[38] J. Huang, S. Rauscher, G. Nawrocki, T. Ran, M. Feig, B.L. de Groot, H. Grubmüller, A.D. MacKerell, CHARMM36m: an improved force field for folded and intrinsically disordered proteins, Nat. Methods 14 (2017) 71–73, https://doi.org/10.1038/nmeth.4067.
[39] B.R. Brooks, C.L. Brooks III, A.D. Mackerell Jr., L. Nilsson, R.J. Petrella, B. Roux, Y. Won, G. Archontis, C. Bartels, S. Boresch, A. Caflisch, L. Caves, Q. Cui, A. R. Dinner, M. Feig, S. Fischer, J. Gao, M. Hodoscek, W. Im, K. Kuczera, T. Lazaridis, J. Ma, V. Ovchinnikov, E. Paci, R.W. Pastor, C.B. Post, J.Z. Pu, M. Schaefer, B. Tidor, R.M. Venable, H.L. Woodcock, X. Wu, W. Yang, D.M. York, M. Karplus, CHARMM: The biomolecular simulation program, J. Comput. Chem. 30 (2009) 1545–1614. https://doi.org/10.1002/jcc.21287.
[40] J. Lee, X. Cheng, J.M. Swails, M.S. Yeom, P.K. Eastman, J.A. Lemkul, S. Wei, J. Buckner, J.C. Jeong, Y. Qi, S. Jo, V.S. Pande, D.A. Case, C.L.I.I.I. Brooks, A.D.Jr. MacKerell, J.B. Klauda, W. Im, CHARMM-GUI Input Generator for NAMD, GROMACS, AMBER, OpenMM, and CHARMM/OpenMM Simulations Using the CHARMM36 Additive Force Field, J Chem Theory Comput 12 (2016) 405–413. https://doi.org/10.1021/acs.jctc.5b00935.
[41] D.R. Roe, T.E.I.I.I. Cheatham, PTRAJ and CPPTRAJ: Software for Processing and Analysis of Molecular Dynamics Trajectory Data, J Chem Theory Comput 9 (2013) 3084–3095. https://doi.org/10.1021/ct400341p.
[42] W.L. Delano, The PyMOL Molecular Graphics System, De-Lano Sc, San Carlos, CA, 2002 http://www.pymol.org.